Siripong Malasri, Ph.D., P.E., CPLP Technologist
Editor-in-Chief, International Journal of Advanced Packaging Technology
Healthcare Packaging Consortium, Christian Brothers University, 650 East Parkway South,
Memphis, TN 38104, USA. Phone 1-901-321-3419; Fax 1-901-321-3402; Email pong@cloud-

Date: January 1, 2014

Dear Readers:

The International Journal of Advanced Packaging Technology is entering its second year of existence. We continue to create a free, valuable resource to the worldwide packaging community via the open access concept.

There will be two sections of Volume 2, Number 1 of the journal. The first section will feature transport packaging articles while the second section will highlight the work in other areas of packaging. Distribution is fundamental to all types of packaging; therefore, we will make a special section on transport packaging. I would like to thank the members of the editorial team for their willingness to work on the Special Issue on Transport Packaging: Theory & Practice. Their names are listed in the Call for Papers for the special issue.

On behalf of the journal, I would like to invite packaging researchers and professionals to share their knowledge by submitting articles for review. All packaging related topics are welcome.

Sincerely,

S. Malasri

Siripong Malasri, Ph.D., P.E., CPLP Technologist
Director, Healthcare Packaging Consortium
Editor-in-Chief, *International Journal of Advanced Packaging Technology*

Cloud Publications
International Journal of Advanced Packaging Technology
2014, Volume 2, Issue 1, pp. 60-69, Article ID Tech-231
ISSN 2349 – 6665, doi 10.23953/cloud.ijapt.15

Case Study | Open Access

Time-Frequency Analysis of Shock and Vibration Measurements Using Wavelet Transforms

Divya Choudhary, Siripong Malasri, Mallory Harvey, and Amanda Smith

Healthcare Packaging Consortium, Christian Brothers University, 650 East Parkway South, Memphis, TN, USA

Correspondence should be addressed to Divya Choudhary, dchodhry@cbu.edu

Publication Date: 21 January 2014

DOI: https://doi.org/10.23953/cloud.ijapt.15

Abstract This article presents the use of the Continuous Wavelet Transform (CWT) for the analysis of shock and vibration measurements. Acceleration measurements from pallets dropped from five different heights and vibration measurements of pallets are acquired in controlled laboratory settings. Power spectral density (PSD) as estimated from CWT is compared to the Shock Response Spectrum as well as the PSD estimated from Fourier Transform (FT) and Short Time Fourier Transform (STFT). CWT overcomes the drawbacks of Fourier Transform in analyzing non-stationary signals such as shock and vibration data. CWT also provides more improved time-frequency resolution than STFT. The article presents results that indicate that CWT can be used as an effective spectral analysis tool for shock and vibration measurements.

Keywords *Continuous Wavelet Transform; Fourier Transform; Shock Response Spectrum; Vibration*

1. Introduction

Packaged products often undergo shock and vibration during distribution. An accurate simulation of the shock and vibration phenomenon enables effective testing of packaging components and provides direction for further improvement of packaging and transportation design. For this purpose, understanding the spectral (frequency) components that are present as a result of stimulus caused by shock and vibration is important. A commonly used spectral analysis tool in the area of signal processing is the Power Spectral Density (PSD). Conventional PSD is computed using the Fourier Transform (FT) which assumes that any signal is composed of a weighted summation of sinusoids of various frequencies [1]. For the signal being analyzed, the PSD represents the power associated with each of these sinusoids. The draw back in the use of PSD based on FT is its inability to accurately represent signals that are non-stationary [2]. Non-stationary signals contain different

frequency components at different periods of time. Shock is a transient event defined as a mechanical disturbance characterized by a rise and decay of acceleration in a short period of time, while vibrations are random oscillations about a reference point, usually for a longer period of time [3]. Given the definitions and observations made through measurements, shock and vibration are considered non-stationary processes. Short Time Fourier Transform (STFT) attempts to address non-stationarity by estimating the spectral content of the signal over small segments of the signals using a sliding window. However, the time-frequency uncertainty principle limits the accuracy of STFT. The Shock Response Spectrum (SRS) is another approach to analyze shock data that assumes a model containing a set of single degree-of-freedom, mass-damper-spring oscillator subsystems that are excited by base motion [4]. For each subsystem, the natural frequency and maximum amplitude of response is determined [3]. The plot of maximum amplitude versus natural frequency is the SRS. Although originally developed for transients associated with shock, SRS is also used for analysis of vibration [5]. Wavelet Transform maps a temporal signal on to a 3-D time-frequency space and is used extensively to analyze non stationary signals [6, 7]. In this article, a technique applying Continuous Wavelet Transform (CWT) is used for spectral analysis of shock and vibration. The technique measures the PSD based on the CWT coefficients. CWT accounts for the non-stationary properties of shock and vibration by not only computing the frequency components present in the signal, but it also computes the time intervals when those frequencies are present. The time-frequency localization properties of wavelet basis functions in conjunction with the mechanism of the transform process, makes CWT an extremely effective spectral analysis tool.

The subsequent sections in this article are as follows: In section 2, data collection methods, signal processing algorithms and software tools are described. Section 3 discusses the results of the analysis of the data and section 4 presents the conclusions drawn from this research.

2. Materials and Methods

In this section, first, a description of the shock and vibration experiment is provided. Next, the signal processing techniques including FT, STFT, CWT, PSD and SRS for analyzing the data are presented. Finally, the software tools to implement the analysis are discussed.

2.1. Data Collection Procedure

For recording shock data, a Lansmont Saver 3M30 recorder was used to measure acceleration versus time at 1000 samples/sec along three directions. It was attached to a pallet, which was raised and dropped from a certain height. In this experiment, a wooden pallet was dropped from 2 inches, 4 inches, 6 inches, 8 inches and 10 inches. Figure 1 shows the setup of the shock experiment. For each height, acceleration versus time was measured through the three channels of the shock recorder. Channel 3 measured the acceleration along the direction of the drop, while the other two channels measuring acceleration along the other two orthogonal directions. For measuring vibrational data, a wooden pallet was mounted on a vibration platform as shown in Figure 2. The Lansmont recorder was used to measure the vibrational acceleration versus time signal sampled at 1000 samples/sec along three orthogonal directions (x, y and z axis). A truck vibration simulation in accordance with ASTM D 4169 Truck Level I was utilized.

Figure 1: *Experimental Setup for Collection of Shock Data*

Figure 2: *Experimental Setup for Collection of Vibration data*

2.2. Signal Processing/Modeling Techniques

In this sub-section, the theoretical background and software tools to compute FT, STFT, CWT as well as the calculation of PSD for each of the stated signal processing technique are presented. In the context of this article, the time varying function $x(t)$ represents the acceleration versus time signal associated with the shock or vibration data. Further, the signal $x(t)$ is normalized by subtracting its mean value from the signal. The mean value corresponds to the zero frequency or the DC component. Thus the normalization prevents the possibility of the zero frequency component from dominating the PSD plots shown in this article. This typically improves clarity of the figures without loss of relevant information.

2.2.1. Fourier Transform

Fourier Transform of a temporal signal $x(t)$ is given by [8]: $X(f) = \int_{-\infty}^{\infty} x(t)e^{-j\omega t}dt$, where $\omega = 2\pi f$ and *j* is the complex number $\sqrt{-1}$. $X(f)$ is the representation of the signal $x(t)$ in the Fourier or

frequency domain. Fourier transform expresses the signal $x(t)$ as a weighted sum of the basis function: $e^{-j\omega t} = cos(\omega t) + jsin(\omega t)$. The equation can be interpreted as follows. Fourier transform in essence decomposes the signal $x(t)$ into constituent sinusoids and the transform finds amplitude and phases of these constituent sinusoids. For a specific value of ω, the signal $x(t)$ is correlated with the basis function: $cos(\omega t) + jsin(\omega t)$. The complex correlation coefficient obtained for that value of ω is the corresponding Fourier Transform coefficient. The complex coefficient represents the amplitude and phase of the sinusoid of frequency ω. This process is repeated for values of ω ranging from $-\infty$ to ∞.

2.2.2. Short Time Fourier Transform

The Short Time Fourier Transform (STFT) is a modification of the conventional Fourier Transform. In STFT, the time domain signal, $x(t)$, is broken into segments. Fourier Transform of each of these segments is the STFT. The process of dividing $x(t)$ into segments is achieved by multiplying the signal with a sliding window function $g(t-\tau)$. The parameter $\mp\tau$ controls the shift or the slide of the window *g(t)* . In this research, a Hanning window of size 10 was used to represent *g(t)*.

STFT of a signal $x(t)$ is given by [9]: $X(\tau,\omega) = \int_{-\infty}^{\infty} x(t)g(t-\tau)e^{-j\omega t}dt$, where $\omega = 2\pi f$ is frequency in radians/second. The plot of STFT coefficients for the signal $x(t)$ is a 3D plot with the x-axis representing the time shift $\mp\tau$ and frequency represented on the y-axis. The amplitude of the STFT coefficients is represented on the z-axis.

2.2.3. Continuous Wavelet Transform

Wavelet Transform represents a signal $x(t)$ as a weighted sum of basis functions referred to as wavelets. The weights correspond to the wavelet coefficients. The Continuous Wavelet Transform (CWT) of a signal $x(t)$ is given by [10]: $X(\tau,s) = \int x(t)\frac{1}{\sqrt{s}}\phi^*\left(\frac{t-\tau}{s}\right)$, where τ is the translation parameter and s is the scale parameter. The basis function $\phi(t)$ is referred to as a mother wavelet. $\phi^*(t)$ is the complex conjugate of $\phi(t)$. The translation parameter, τ, shifts $\phi(t)$ in time and the scale parameter, *s,* controls the temporal width of $\phi(t)$. The scale parameter is inversely related to frequency. An example of a mother wavelet function is a Morlet function. The Morlet wavelet is a complex valued function given by: $\phi(t) = e^{-2\pi^2\frac{t^2}{z_0^2}}\left(e^{j2\pi t} - e^{2\pi^2 t^2}\right)$. The envelope factor z_o controls the number of oscillations in the wavelet with a typical value of z_o = 5 [11]. The Morlet basis function is used in this article for the computation of CWT.

The CWT, in simpler terms, is the correlation of the signal $x(t)$ with various shifted and stretched/shrunken versions of the mother wavelet $\phi(t)$. It is this ability to manipulate the width (stretching or shrinking) of the mother wavelet and shift it along the time axis that makes the CWT time-frequency analysis effective. The plot of CWT coefficients for the signal $x(t)$ is a 3D plot. The x-axis corresponds to the time shift, $\mp\tau$. The y-axis represents frequency *f* or scale *s*. The amplitude of the CWT coefficients is represented by the z-axis.

2.2.4. Power Spectral Density

Power Spectral Density (PSD) of a signal represents the distribution of power over various frequencies that compose the signal. It is the average or expected value of the Fourier Transform of the signal $x(t)$ computed over an infinite time period. PSD of a signal $x(t)$ is given by:

$$S_x(f) = \lim_{T\to\infty} E\left\{\frac{1}{2T}\left|X(f)\right|^2\right\} = \lim_{T\to\infty} E\left\{\frac{1}{2T}\left|\int_{-T}^{T} x(t)e^{-jwt}\,dt\right|^2\right\}$$

T refers to the period over which the statistical average *E{}* of the Fourier Transform, *X(f),* is computed. The above equation can be implemented using computer algorithms based on techniques such as the Welch's Method. Welch's method computes the PSD of a digitized signal $x[i]$ using the following steps [12]:

- Partition the signal $x[i]$ in K overlapping segments, each of length *L,* with M points overlapping between adjacent segments.

- Next, each segment, $x_k[i]$, is multiplied by a window function W and the modified periodogram is computed using an N-point Discrete Fourier Transform (DFT) as shown in equation below.

$$A_k(n) = \frac{1}{L}\sum_{i=0}^{L-1} x_k(i)W(i)e^{\frac{-2\pi in}{L}}$$

  Here *n* = 0, 1, 2, ... *N*-1 and *k* = 0, 1, 2, ... *K*-1. *N* is the number DFT points and *K* is the number of segments used in partitioning the data, $x[i]$. A particular value of *n* corresponds to a frequency $f_n = \frac{nf_S}{N}$, where f_S is the sampling frequency of the signal. An example of a window function is:

$$W(i) = 1 - \left[\frac{i - \frac{L-1}{2}}{\frac{L+1}{2}}\right]^2$$

- The PSD is then estimated using the equation

$$\hat{S}_x(f_n) = \frac{L}{UK}\sum_{k=1}^{K}\left|A_k(n)\right|^2,$$

  Where, $U = \frac{1}{L}\sum_{i=0}^{L-1} W^2(i)$

The implementation of DFT is commonly done using the Fast Fourier Transform. PSD based on STFT and CWT is estimated by simply computing the magnitude squared of the respective transform coefficients. In this article, with regard to the PSD plots shown in the results section, FT based plots are 2-D figures with PSD on the y-axis and frequency on the x-axis. PSD from STFT and

CWT are 3-D figures with PSD on the z-axis, while time and frequency are on the x and y axes respectively.

2.2.5. Shock Response Curve

In order to compute the Shock Response Curve (SRS), it is assumed that the system is composed of a set of single degree-of-freedom oscillator subsystems. Each subsystem has its own frequency response that peaks at its natural frequency. The acceleration versus time data measured from a shock or vibration experimentation is then filtered by using the frequency response of the SDOF subsystems. The maximum amplitude at the output of the filtering processing for each SDOF subsystem is noted. SRS is a plot of the maximum amplitude versus the natural frequency of each of the SDOF subsystem [13].

2.3. Software Analysis Tools

The shock and vibration data collected in the experiments are processed using Matlab programming language to compute PSD from FT using Welch's Method, STFT and CWT. SRS was computed using software developed by Tom Irvine based on the Kelly Richman algorithm [14, 15].

3. Results and Discussion

Figure 3 shows the acceleration, PSDs and SRS for the shock experiment for a 2 inch drop along the direction of the drop (z axis). Figure 4 shows the acceleration, PSDs and SRS for the vibration experiment along the z axis. Figures 3 and 4 are exemplar plots and the observations derived through these are consistent for other measurements from the experiment as well. A caveat needs to be pointed out about SRS. SRS is calculated by computing the maximum amplitude of the response for a set of SDOF oscillators. Hence, the motivation and mathematical background associated with SRS is different from that of other signal processing techniques used in this article. In comparing the various techniques, it can be observed that PSD from FT and SRS are 2-D plots that represent frequency domain information about the signal and do not capture temporal information. The PSD from STFT and CWT are 3-D plots that capture both temporal and frequency domain information. All the techniques identify the dominant frequency at about 75 Hz. For FT based PSD and SRS, there is no information about the time periods when these frequencies are present. Both STFT and CWT indicate that the dominant frequency component occurs approximately in a temporal region around 0.2 seconds. Uncertainty principles in time-frequency resolution dictates that the time instant when a specific frequency signal occurred can only be estimated up to certain accuracy. This means that temporal accuracy is always gained at the cost of losing frequency localization and vice versa. STFT shown in Figure 3 was computed with high temporal resolution. As a result, the frequency resolution of STFT is compromised and this is represented by the exaggerated presence of frequency components in the 100 Hz - 200Hz range. If STFT were to be computed with emphasis on frequency resolution, the temporal resolution would be lost and localization along the temporal axis would deteriorate. On the other hand, by controlling the scale and the shift parameters of the wavelet basis function for computing the transform, PSD from CWT innately balances both temporal and frequency resolutions. This is apparent from the CWT PSD in Figure 3, which shows better localization along the time and frequency axis around 0.2 seconds and 75Hz (the dominant frequency). The presence of these frequencies is also noticed, with lower power, around 0.3 seconds in both CWT and STFT. Similarly, inferences can be made for vibrational data analysis as represented in Figure 4. The vibrational data analysis shows strong frequency components in the frequency band less than 100 Hz. CWT and STFT show that these frequency components occur around 0.1 seconds and 0.2 seconds. Given the advantages in terms of time-frequency representations of STFT and CWT, both techniques, however, are computationally challenging when compared to FT. An alternative to CWT is the discrete wavelet transform (DWT). It

should be noted that the disadvantage with DWT is that, in order to achieve computational efficiency, DWT uses truly discrete time and frequency locations in its computations by algorithmically skipping certain locations on the time-frequency plots. This makes DWT plots less intuitive for visualization and interpretation in its raw form.

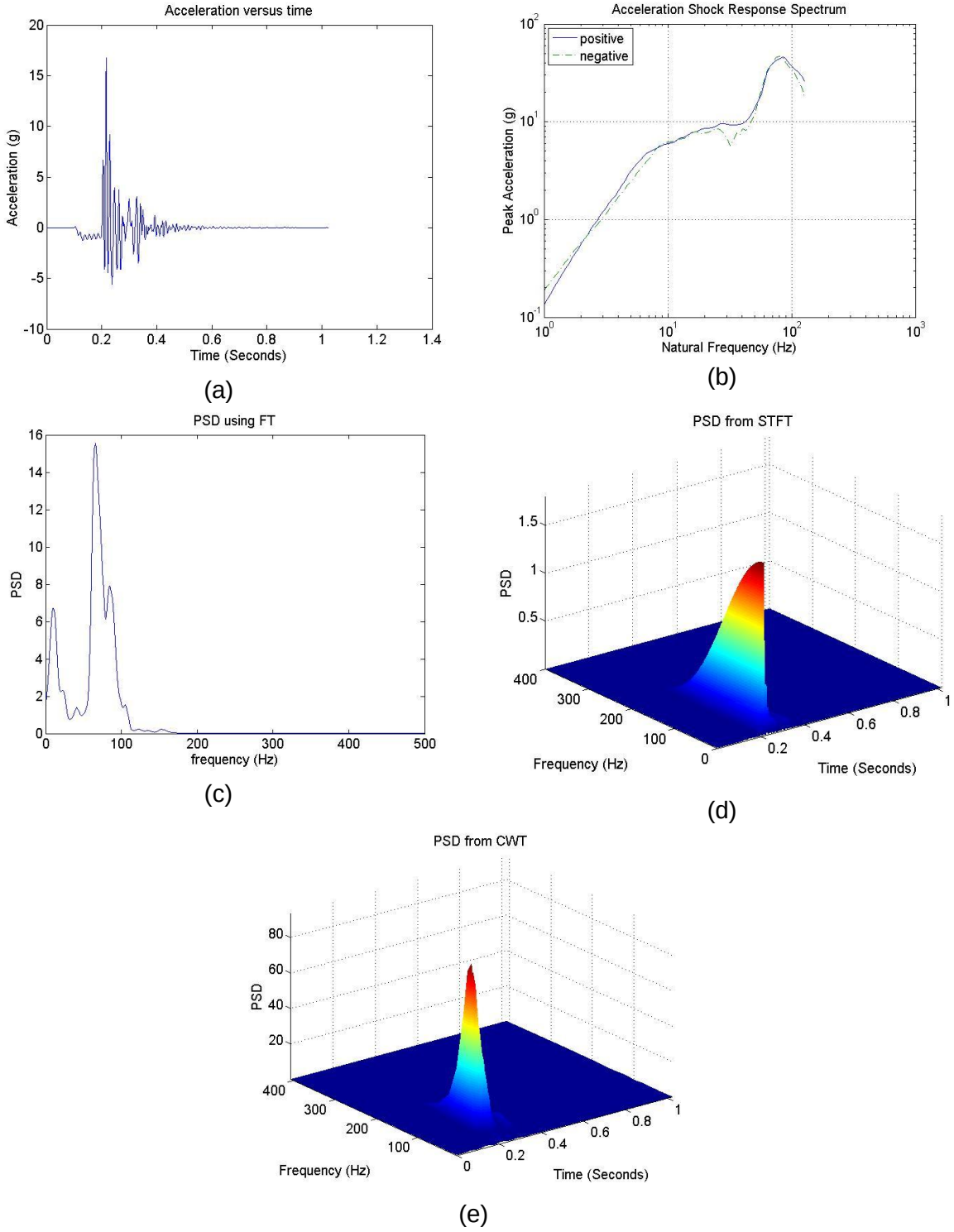

***Figure 3**: Data Measurement and Analysis for 2 Inch Pallet Drop Measured in the Direction of the Drop. Shock Acceleration versus Time Measurement (a), SRS (b), PSD from FT (c), PSD from STFT (d), and PSD from CWT (e)*

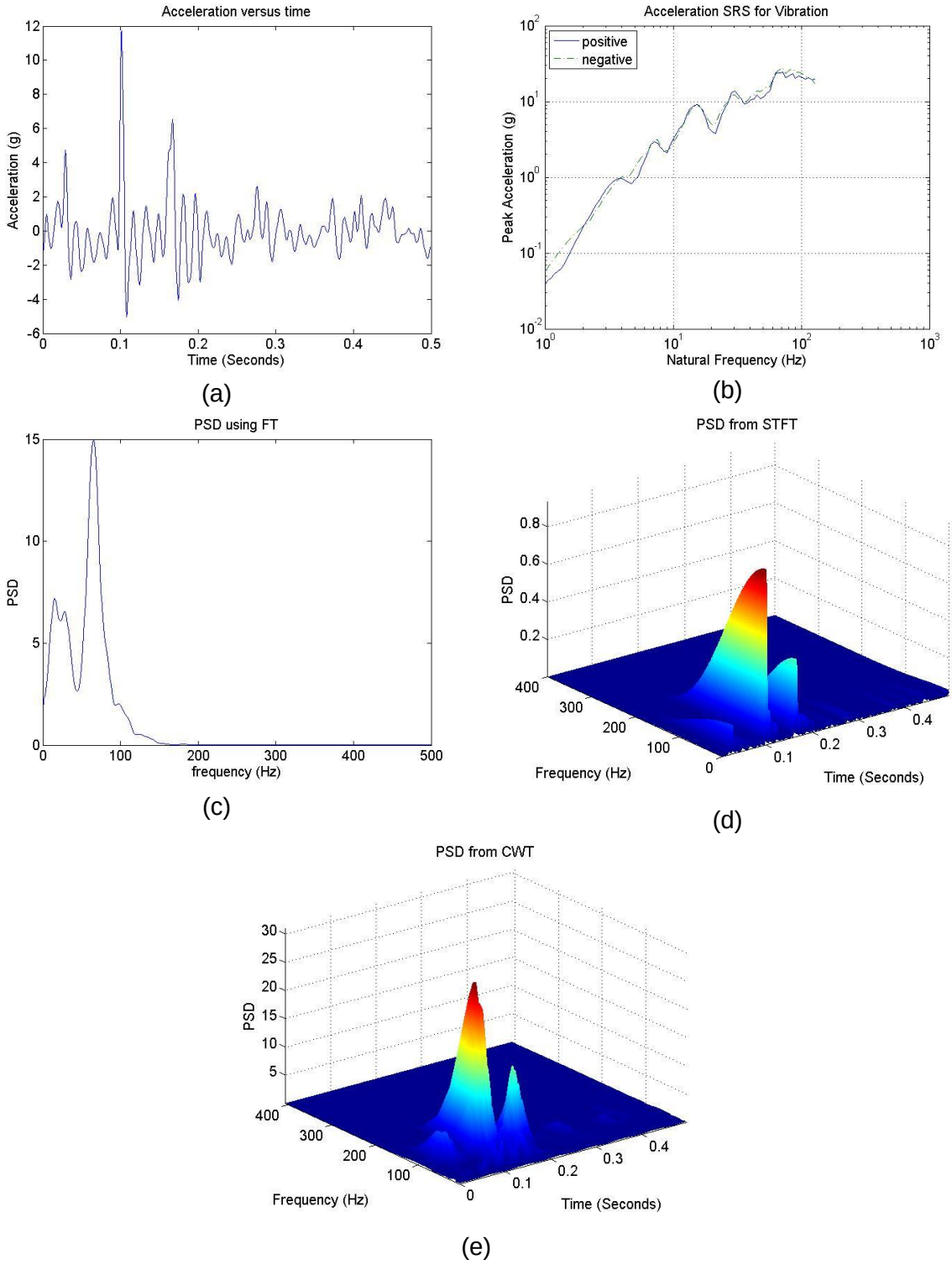

Figure 4: *Data Measurement and Analysis of Vibration along the Z-Axis. Vibrational Acceleration Versus Time Measurement (a), SRS (b), PSD from FT (c), PSD from STFT (d), PSD from CWT (e)*

4. Conclusion

The focus of this article was to present CWT as a tool to analyze the time-frequency characteristics of shock and vibration and compare its analytical effectiveness to conventional techniques such as

SRS and PSD based on FT. In a controlled laboratory setting, acceleration of wooden pallets associated with shock and vibration was measured. PSD based on FT, STFT and CWT was computed. SRS was also calculated from the shock and vibrational data. Results of the analysis show that CWT has the ability to provide optimum joint frequency and time resolution. In using STFT there is a tradeoff between temporal and frequency resolutions. FT provides solely frequency domain representation of the signal with no information about time periods when the frequency components occur. SRS on the other hand provides a plot of maximum amplitude response versus natural frequencies by assuming a set of subsystems with SDOF. This article concludes that with the ability to present both time and frequency information with optimum localization, CWT is an effective tool for modeling non-stationary signals such as shock and vibration.

References

[1] Semmlow J., 2011: *Signals and Systems for Bioengineers: A Matlab Based Approach*. Academic Press, 604.

[2] CEEES Technical Advisory Board for Mechanical Environments, 2008: *A Review of Methodologies for Deriving Vibration and Shock Test Severities*. 28.

[3] Kipp, W., 1998: *PSD and SRS in Simple Terms*. ISTA Conference, Orlando, FL.

[4] Hollowell B. and Smith S. *A Proposed Method to Standardize Shock Response Spectrum (SRS) Analysis*. International Environmental Science and Technology Journal. 1996. 39 (3) 19-24.

[5] Brandt A., 2011: *Noise and Vibration analysis: Signal Analysis and Experimental Procedures*. Wiley, 464.

[6] Pittner S. and Kamarthi S. *Feature Extraction for Wavelet Coefficients for Pattern Recognition Tasks*. IEEE Transactions on Pattern Analysis and Machine Learning. 1999. 21 (1) 83-88.

[7] Usner M. and Aldroubi A. *A Review of Wavelets in Biomedical Applications*. Proceedings of IEEE. 1986. 84 (4) 626-638.

[8] Roberts M., 2003: *Signals and Systems, Analysis of Signals through Linear Systems*. McGraw-Hill, 1054.

[9] Marks R., 2009: *Handbook of Fourier Analysis and Its Applications*. Oxford University Press, 800.

[10] Mallat S., 2009: *A Wavelet Tour of Signal Processing: A Sparse Way*. 3rd Ed. Academic Press, 832.

[11] Lewalle J. and Keller D., 2005: *Analysis of Web Defects by Correlating 1-D Morlet and 2-D Mexican Hat Wavelet Transforms*. Proc. of SPIE, Wavelet Applications in Industrial Processing III, 63-74, Boston, MA.

[12] Welch, P.D. *The Use of Fast Fourier Transform for the Estimation of Power Spectra: A Method Based on Time Average Over Short, Modified Periodogram*. IEEE transactions on Audio and Electroacoustics. 1967. AU-15, 70-73.

[13] Halfpenny, A., (As of December 31, 2013): *Accelerated Vibration Testing Based on Fatigue Damage Spectra.* http://www.ncode.com/fileadmin/mediapool/nCode/downloads/Whitepaper_nCode_AHP_AcceleratedVibrationTestingBasedonFatigueDamageSpectra_v2-Halfpenny.pdf.

[14] Kelly R. and Richman G., 1969: *Principles and Techniques of Shock Data Analysis: Shock and Vibration Monograph*, 5, Shock and Vibration Information Center, United States Department of Defense, Washington D.C., 1-197.

[15] Irvine T., 2006: *Shock Response Spectrum*. http://www.mathworks.com/matlabcentral/fileexchange/7398-shock-response-spectrum/content/srs.m.

Cloud Publications
International Journal of Advanced Packaging Technology
2014, Volume 2, Issue 1, pp. 70-74, Article ID Tech-232
ISSN 2349 – 6665, doi 10.23953/cloud.ijapt.16

Trends Article

Open Access

Trends in Distribution Simulation Testing

Eric Joneson

Lansmont Corporation, 17 Mandeville Court, Monterey, California, USA

Correspondence should be addressed to Eric Joneson, eric_joneson@lansmont.com

Publication Date: 13 February 2014

DOI: https://doi.org/10.23953/cloud.ijapt.16

Abstract Packaged-product distribution simulation tests are most effective when the damage assessment made from actual supply chain and after laboratory testing achieves high correlation. In order to create effective distribution tests, clear understanding of the distribution environment must be developed and documented. This can be achieved by "*walking the system*"; making direct observations from within various distribution channels. Challenges associated with thorough and complete supply chain access limits the overall effectiveness of walking the system. One way to address those challenges is to use non-intrusive portable data recorders that can travel within the global supply chain, measuring critical distribution hazards such as shock, vibration, compression, temperature, humidity and other valuable information. This article details trends associated with the growth of advanced simulation testing based upon measured data from within the supply chain.
Keywords *Distribution; Simulation; Data Recorder; Packaged Products; Vibration Testing*

1. Introduction

Controlled packaged-product distribution testing has been taking place for more than sixty-five years. In the early 40's Westinghouse Electric's major appliance division began vibration and incline impact testing. Because of rising damage levels, the Porcelain Enamel Institute accepted an offer in 1948 from Westinghouse to publish their testing procedures under a banner called the National Safe Transit Committee. In 1958 that committee became known as the NSTC, Inc., and National Safe Transit Association (NSTA) in the mid-1970s, before adding two more test procedures to their offerings in 1984.

Those simple, but effective test procedures are still in use today, however over the past 20 years or so, distribution testing has progressed from what was more general and robust, to more focused and tailored simulation. In the mid-1990s, NSTA's board began to pursue a more global presence due to the changes in the global economy and supply chain. NSTA became the International Safe Transit

Association (ISTA) and since 1996, ISTA has expanded from 4 published US test procedures to 22, developed with global input and performed thousands of times annually around the world.

2. Current and Future Practices of Distribution Simulation Testing

All that new development has taken place in the areas of general and focused simulation, with test procedures for Small Parcel Simulation [1], Club Store Distribution Simulation [2], Fast Moving Consumer Goods [3] and ISTA's 4AB [4], which is a web-based application that allows users to build and select their testing procedures based upon their ability to map out their known distribution channels.

Global sustainability initiatives have demanded more responsible package design, focusing on material reduction, reuse, and recycling. Less packaging is typically considered "better", however reductions of protective packaging may cause more susceptibility to distribution hazards such as shock, vibration or compression. Thorough distribution testing becomes even more critical in qualifying proposed sustainable packaging solutions.

***Figure 1**: Damaged Corrugated Container Due to Reduction in Structural Material Used*

As a rule, distribution testing should be representative of the hazards your products will encounter when moving through the supply chain. The more you know and understand about the hazards in your environment(s), the more likely you'll succeed at protecting against them. Lack of knowledge causes one to err on the side of caution. In terms of distribution testing, that means using test procedures that are general in nature, and more robust in their intensity. That may be counterproductive to sustainable packaging initiatives. More robust testing probably requires more (*not less*) packaging materials to adequately protect the product.

***Figure 2**: The More You Know About the Supply Chain, the Better You Can Simulate it in the Lab*

Technological advances and a global thirst for knowledge have facilitated a growing repository of distribution hazard metrics and understanding. Portable data recorders can be configured to capture time-stamped, shock, drop, vibration, force, temperature, humidity and atmospheric pressure data, providing valuable record as to the hazards present within the supply chain. These data recorders are routinely mounted to transport vehicles and within transport packaging, some traveling on 60 day-plus international journeys, all in an effort to document the dynamic and climatic hazards present in any number of distribution channels.

***Figure 3**: Installing a Data Recorder on the Floor of a Truck Trailer for Distribution Measurement*

By developing this clear and concise understanding of ocean, air, truck and even intermodal transport distribution, testing can be developed to simulate those environments. Statistically valid summaries of the data are used to subsequently build handling, storage, transport and even climatic conditioning profiles. ISTA provides its members with documentation, such as their **ISTA Field Data Requirements** (published 2008, revised 2009), intended to give members guidance on how properly configure, record and analyze field data. Using these guidelines, ISTA has created their “Data Depot”, archiving transportation/distribution environment information that they use to develop or enhance their published standards. International research working groups continue to look at improved, consistent methods of capturing this distribution data such that capable instruments can be used globally to develop industry test methods.

As our collective understanding of the distribution environment continues to grow, our ability to simulate those characteristics has improved as well. Measurements made during truck accelerating, braking and turning maneuvers has resulted in both test procedures and laboratory equipment that are used to specifically predict unit load stability. In 2012, The Fraunhofer Institute, located in Dortmund, Germany commissioned Lansmont Corporation to build the first ever, Load Stability test system. The Dortmund based Fraunhofer Institute specializes in research and expertise associated with load securement solutions. It was imperative that their test system possessed the exact time-history characteristics associated with emergency truck maneuvers such as braking, accelerating and turning.

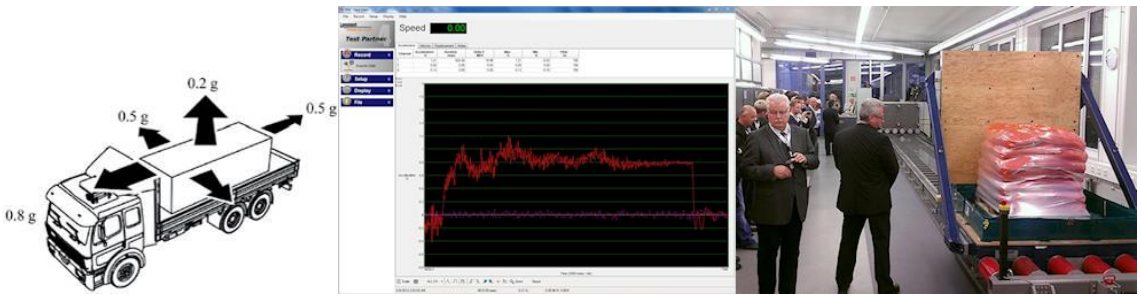

***Figure 4**: (a) Typical Forces Experienced Due to Braking, Accelerating and Turning, (b) Load Stability Test System Installed at Fraunhofer Institute in Dortmund, Germany*

ISTA currently has a Load Stability Workgroup that has been tasked to develop and incorporate the first-ever, specifically targeted load stability tests into their general simulation test series. ISTA members can inquire about opportunities to participate in this Working Group by contacting A.J. Gruber, ISTA's Vice President of Technical, at ajgruber@ista.org.

Concurrently, efforts within ASTM D10 are in process to update the random vibration profiles in D4169 [5]. It's widely accepted that the existing profiles are overly severe and not representative of today's over-the-road, rail or air transport environments. Representative transport data is being analyzed to determine the most relevant spectral shapes, intensities while also addressing overall test duration.

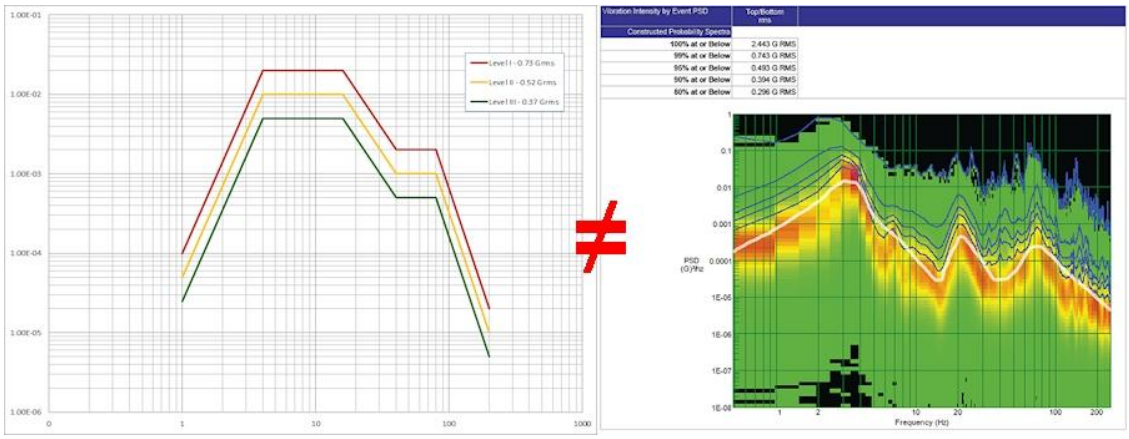

Figure 5: *Comparison of ASTM Truck Spectra (Levels 1-3) and Recently Measured Vibration Spectra from Multiple Over-The-Road Truck Trailer Shipments*

Other groups such as the Distribution Working Group within the International Association of Packaging Research Institutes (IAPRI) [6] continue with their efforts to document advanced vibration testing methodologies, such as time-history replication and multi-axis testing. Trucks and trains shake not only up-and-down, but also side-to-side, while rolling back and forth and pitching forward and backward. If packaged products are susceptible to those dynamics, it might make sense to selectively use that field measured data to drive that appropriate method of testing in the laboratory.

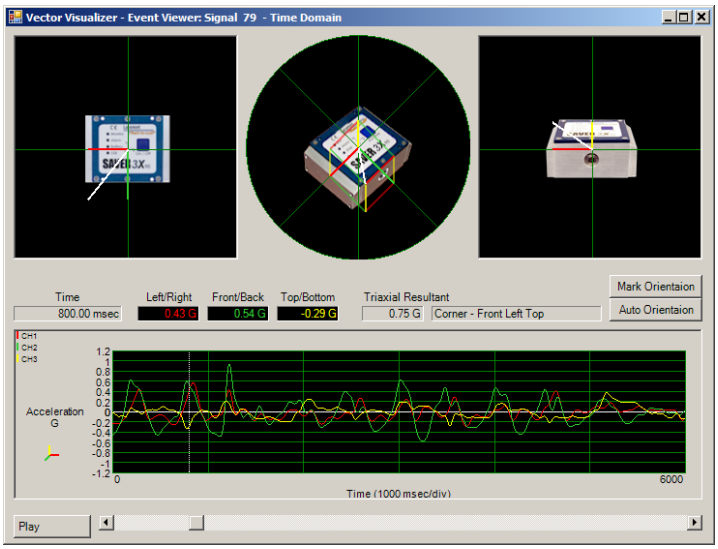

Figure 6: *Measured Time-History Event, Showing the Multi-Axis Energy Characteristics of the Event Itself*

Medical and pharmaceutical packaged products must comply with regulatory requirements that provide general, but stringent guidance, dictating “Each manufacturer shall ensure that device packaging and shipping containers are designed and constructed to protect the device from alteration or damage during the customary conditions of processing, storage, handling, and distribution” [7]. Many medical device and pharmaceutical manufacturers have consequently found it in their best interest to prove that their packaged-product testing practices are representative of the real world, by establishing measured, defendable evidence of their test procedure development process.

3. Conclusion

A documented, comprehensive understanding of specific distribution channels can provide the ability to tailor packaged-product distribution simulation such that any damage assessment performed after laboratory testing will achieve better correlation with results as measured from within the supply chain. Global, relevant testing organizations such as ISTA and ASTM are focusing their development efforts on advanced simulation tests, reducing the levels of over-testing that is generally accepted to be prevalent in many current, common test procedures.

References

[1] ISTA Procedure 3A, 2008: Packaged-Products for Parcel Delivery System Shipment 70 kg (150 lbs.) or Less, International Safe Transit Association, East Lansing, MI.

[2] ISTA Project 6-SAMSCLUB, 2010: Packaged-Products for Sam’s Club® Distribution System Shipment, International Safe Transit Association, East Lansing, MI.

[3] ISTA Project 3K, 2011: Fast Moving Consumer Goods in the European Retail Supply Chain, International Safe Transit Association, East Lansing, MI.

[4] ISTA Procedure 4AB, 2009: Packaged-Products for Shipment in Known Distribution Channels, International Safe Transit Association, East Lansing, MI.

[5] ASTM Standard D4169, 2008: Standard Practice for Performance Testing of Shipping Containers and Systems. ASTM International, West Conshohocken, PA.

[6] International Association of Packaging Research Institutes (IAPRI), www.iapri.org, as of January 13, 2014.

[7] Code of Federal Regulations (CFR) Part 820, Section 130 – Device Packaging, as of January 13, 2014.

Cloud Publications
International Journal of Advanced Packaging Technology
2014, Volume 2, Issue 1, pp. 75-83, Article ID Tech-239
ISSN 2349 – 6665 doi 10.23953/cloud.ijapt.9

Research Article **Open Access**

Measurement and Analysis of Vehicle Vibration for Bottled Water Delivery Trucks

Kyle Dunno

Department of Food, Nutrition, and Packaging Sciences, Clemson University, Clemson, South Carolina, U.S.

Correspondence should be addressed to Kyle Dunno, kdunno@clemson.edu

Publication Date: 18 March 2014

DOI: https://doi.org/10.23953/cloud.ijapt.9

Abstract A bottled water delivery truck was instrumented with a field data recorder to analyze the vibration inputs experienced by the freight holding area of the vehicle. Three delivery routes were chosen for this study–rural delivery, highway delivery, and inter-city delivery. Statistically there were no differences between the generated PSD profiles produced from the study, but it was determined the inter-city delivery had the highest overall Grms of the three delivery routes analyzed.
Keywords *Vehicle Vibration; Delivery Truck; Vibration Testing; PSD Profiles*

1. Introduction

Packaged products are transported via multiple distribution channels to reach their specified destinations. Throughout the various distribution channels, the packaged products are subjected to three major categories of dynamic hazards: shock, vibration, and compression [1]. While shock and compression hazards cannot be overlooked when designing packages or packaging materials, the basis of this research focuses on vibration, specifically beverage delivery truck vibration. The nature and intensity of vibration experienced by a packaged product depends on the type of transportation used. Different modes of transport produce different vibration inputs to the packaged product system.

This study evaluated three different types of delivery locations for bottled water. For the purpose of this paper they will be classified as rural delivery, highway delivery, and inter-city delivery locations. The rural locations utilized roads containing non-highway routes for delivery. Highway locations utilized a combination of major highways and interstates for delivery. Inter-city locations focused on metropolitan businesses utilizing city roadways. These varying routes were evaluated to determine if there were any significant differences of vibration input for the different delivery locations.

The purpose of the project is to measure and analyze vehicle vibration for 5 gallon bottled water (beverage) delivery vehicles. Previous vehicle vibration studies have focused on over-the-road trailers and local package delivery vehicles (UPS and FedEx), but currently there are no published vibration profiles for beverage delivery vehicles [2]. Figure 1 displays the commonly used vibration power spectral density (PSD) profiles used for analyzing truck vibration as reported by the International Safe Transit Association [3]. It should be noted these are the uncompressed PSD profiles.

ISTA produces test standards and PSD profiles in order to simulate truck vibration. These PSD profiles represent the intensity of vibration that occurs inside the cargo hold of the vehicle where packages are placed during transit [2]. Currently, PSD profiles are used to drive vibration tables in order to simulate a particular vehicle environment. Current data collection techniques for obtaining over-the-road vibration data for a truck require the attachment of a recorder to the floor of the vehicle [4]. Data collected from the recorder is then used to drive vibration tables in order to simulate the recorded environment. Through the use of field data recorders this study aims to characterize the vibration profile of a bottled water delivery vehicle. The benefit of more accurately characterizing a vehicle's vibration response is the improvement of testing standards and the tools for package design.

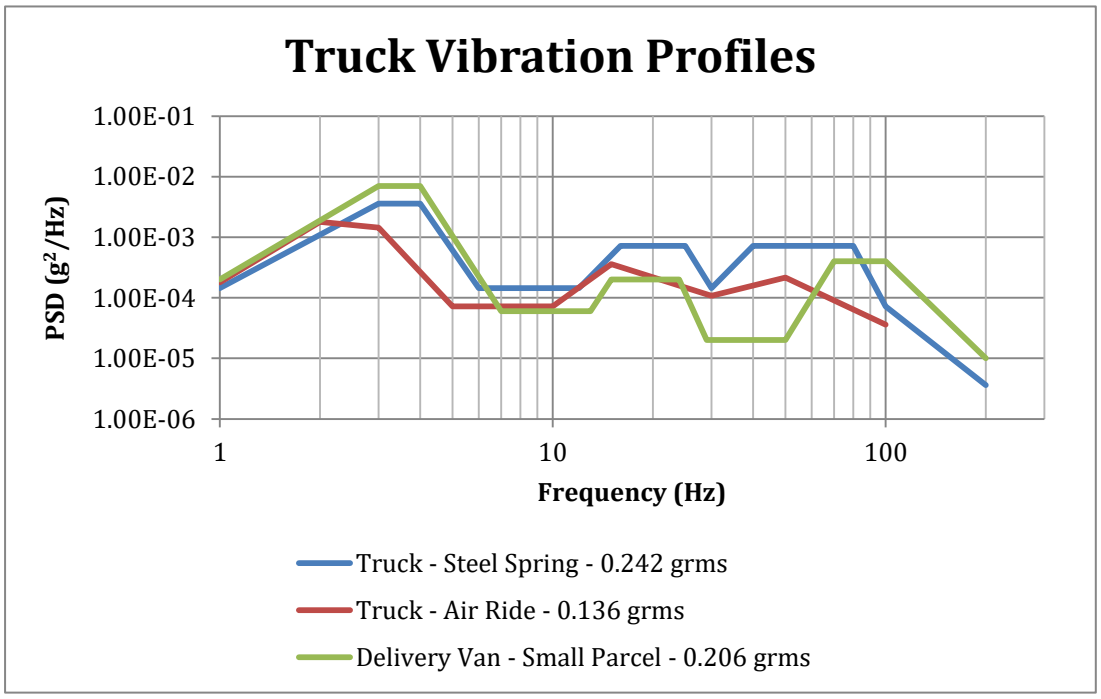

Figure 1: *Commonly Used Vibration Power Spectral Density (PSD) Profiles*

2. Materials and Methods

Shock and Vibration Environment Recorder (SAVER™) (Lansmont Corp., Monterey, CA) model SAVER™ 9X30 with Saver Xware programming software was used in this study. This type of data recorder uses an internal triaxial accelerometer to measure vibration levels in the vertical, lateral, and longitudinal directions. The data recorder was rigidly mounted to the vehicle's chassis just above the rear wheel. Figure 2 illustrates the location of the data recorder.

Figure 2: *Location of the Data Recorder*

The data recorder was programmed to record and analyze vibration using both signal and timer triggered data collecting methods. Signal triggered data refers to the data recorded during an event in which the intensity exceeds a preset threshold. Timer trigger data refers to the data recorder "waking up" at a preset frequency and recording for a preset duration. The following were the recording parameters used for this project:

- Signal Triggered Data
    - Event Trigger Threshold: 0.50 G
    - Sample Rate: 1000 Samples/Sec
    - Record Time: 2.048 sec.
    - Signal Pre-Trigger: 50%
- Timer Triggered Data
    - Wakeup Interval: every 7 min.
    - Sample Rate: 1000 Samples/Sec
    - Record Time: 2.048 sec.

The vehicle used for this study was a 2004 Navistar International 4300 model (Figure 3). Vibration levels were recorded both on signal trigger as well as a fixed interval. The data recorder was turned on prior to the delivery truck leaving the filling location and was turned off once the truck had returned.

For each location, measurements exceeded 20 hours of monitoring for each of the delivery locations. The locations of the study were as follows: Kingsport, TN, Winston-Salem, NC, and Atlanta, GA. The Kingsport, TN location captured the rural delivery routes, the Winston-Salem, NC captured highway delivery, and Atlanta, GA captured inter-city delivery of the bottled water.

Figure 3: *International 4300*

3. Results and Discussion

For each of the three delivery locations, a separate PSD profile was created. Table 1 represents the overall Grms levels for each of the three delivery locations. Each of the PSD profiles (Figures 4-6) shows the results in power density levels versus frequency in the lateral, longitudinal, and vertical axes. The vertical axis produced highest overall Grms values of the three axes, and the inter-city delivery route had the highest overall vertical Grms value of 0.303.

The varying intensity of the Grms values reported in this study match closely with what other researchers have reported in previous studies of inter-city and highway delivery vehicles [5]. The higher Grms values of the inter-city location could be attributed to external sources such as road surface irregularities and repeated braking and forward acceleration [6]. These irregularities and repeated braking and accelerating happen much less frequently in the rural and highway delivery routes of this study resulting in lower overall Grms values.

Table 1: *Overall Grms Values for the Delivery Locations*

Overall Grms Values			
	Rural	**Highway**	**Inter-city**
Longitudinal (x-axis)	0.152	0.144	0.165
Lateral (y-axis)	0.244	0.210	0.277
Vertical (z-axis)	0.280	0.253	0.303

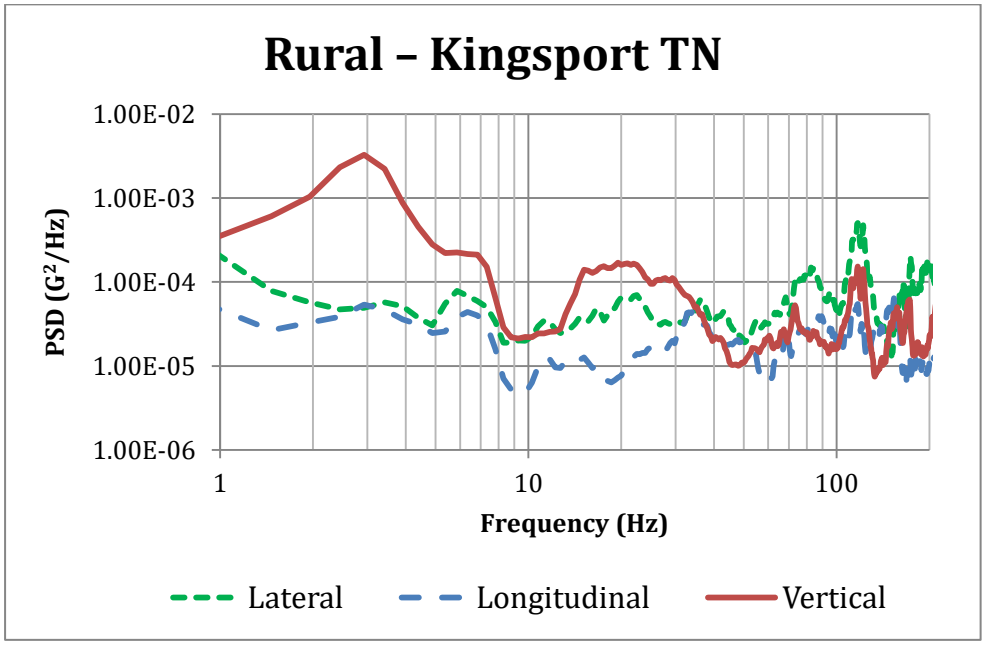

Figure 4: *PSD Profile for Rural Delivery – Kingsport, TN*

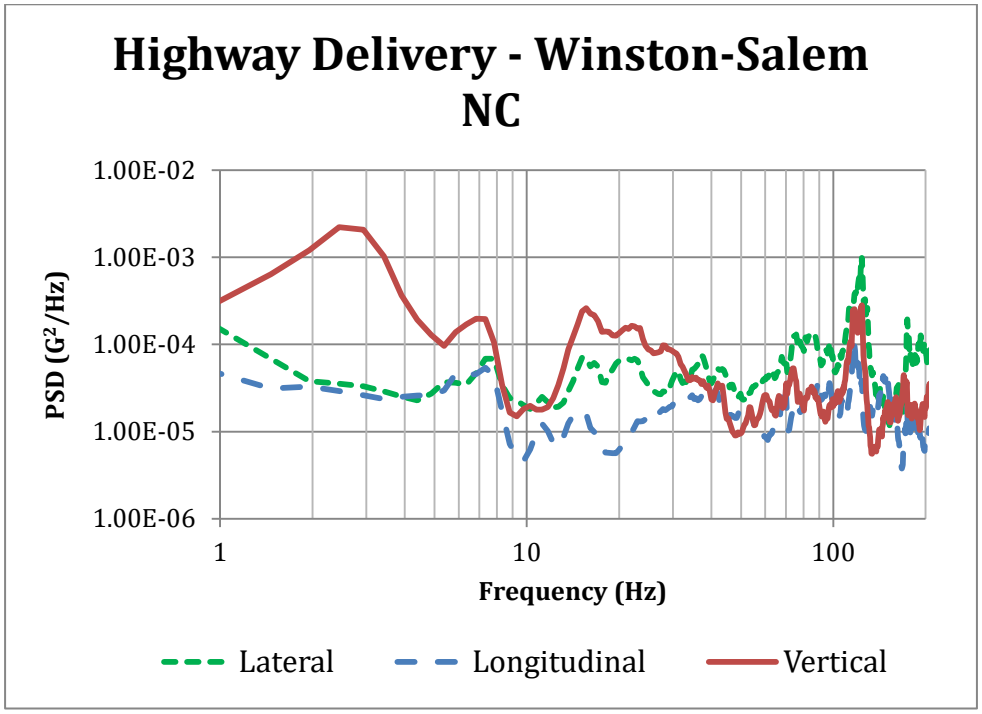

Figure 5: *PSD Profile for Highway Delivery – Winston-Salem, NC*

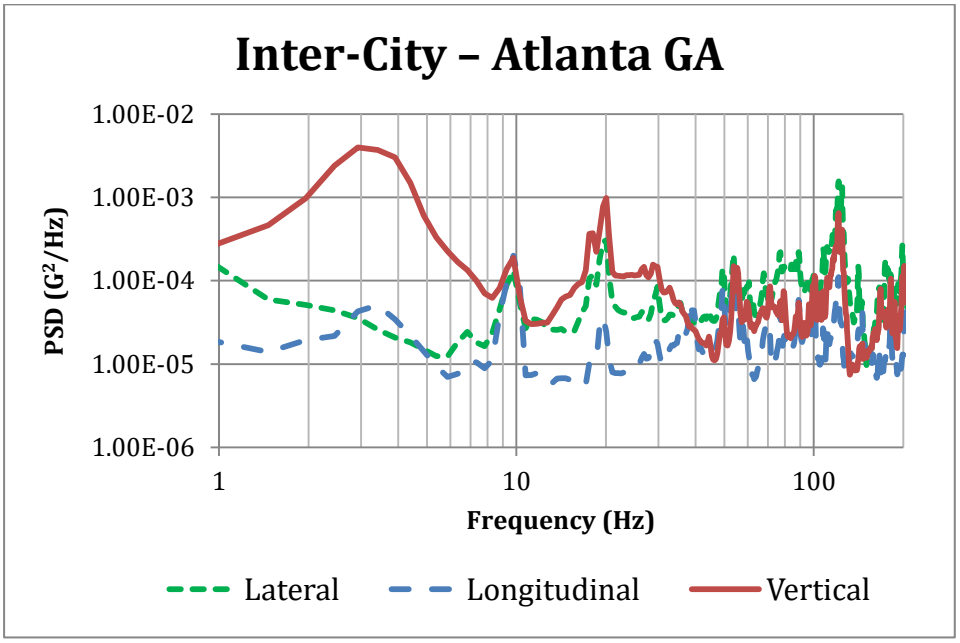

Figure 6: *PSD Profile for Inter-City Delivery – Atlanta, GA*

The vehicle used during this study was a leaf spring style truck. Figure 7 illustrates the results from this study in comparison to the uncompressed ISTA Steel Spring Truck and Delivery Truck profiles. While it is important to consider the overall Grms level of the five PSD profiles, the general shape of the curve should also be evaluated as different peak intensities and frequencies will excite packages and products differently. The results from this study follow closely with the ISTA Steel Spring PSD profile at frequencies less than 10 Hz, but vary significantly between 30-100 Hz. When comparing this study with the ISTA Delivery Truck PSD profile, the shapes of each of the curves follows closely with that of the ISTA profile, except between 50-100 Hz. The energy reported by ISTA is much greater than that reported by this study.

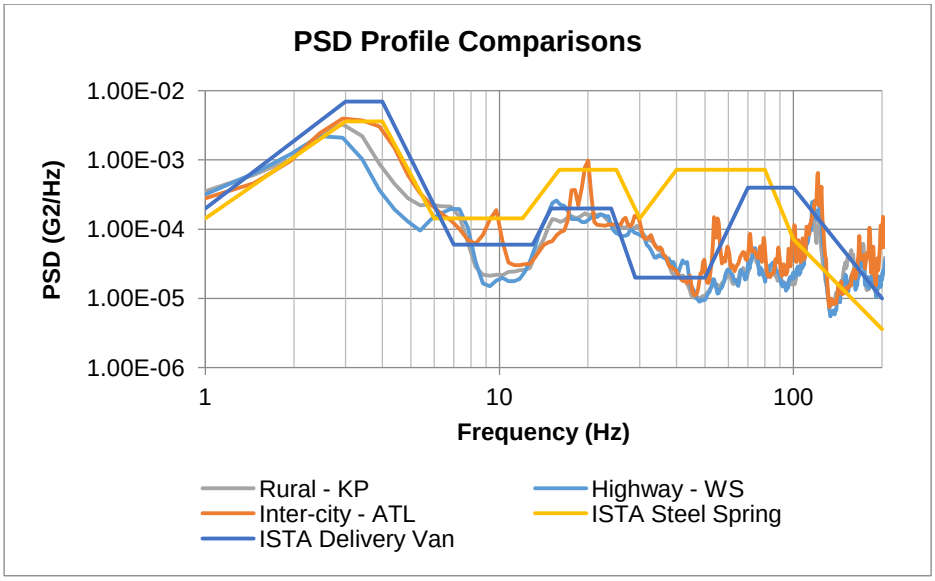

Figure 7*: Comparison of Truck Vibration Profiles*

Table 2 displays the highest overall Grms value for each of the three delivery locations. Overall the highway delivery routes resulted in the lowest overall Grms levels, while the highest overall Grms levels occurred during the inter-city delivery of the bottled water. When the three delivery routes were compared however, there were no statistical differences between the mean overall Grms levels (α=0.05).

Table 2: *Maximum Grms Values for the Delivery Locations*

Maximum Grms Values			
	Rural	**Highway**	**Inter-city**
Longitudinal (x-axis)	0.543	0.498	0.587
Lateral (y-axis)	0.933	0.853	0.979
Vertical (z-axis)	3.234	3.198	4.012

Using the vertical axis results, the data for each delivery location was used to determine the cumulative distribution function (CDF) of the RMS (G) and fitted in a modified Weibull distribution model [7]. The PSD levels shown in Figures 4-6 represent 100% of the CDF. The RMS (G) values were then evaluated to observe the distribution for each delivery location. Histograms containing the frequency and cumulative percentage of the RMS (G) values are presented in Figures 8-10.

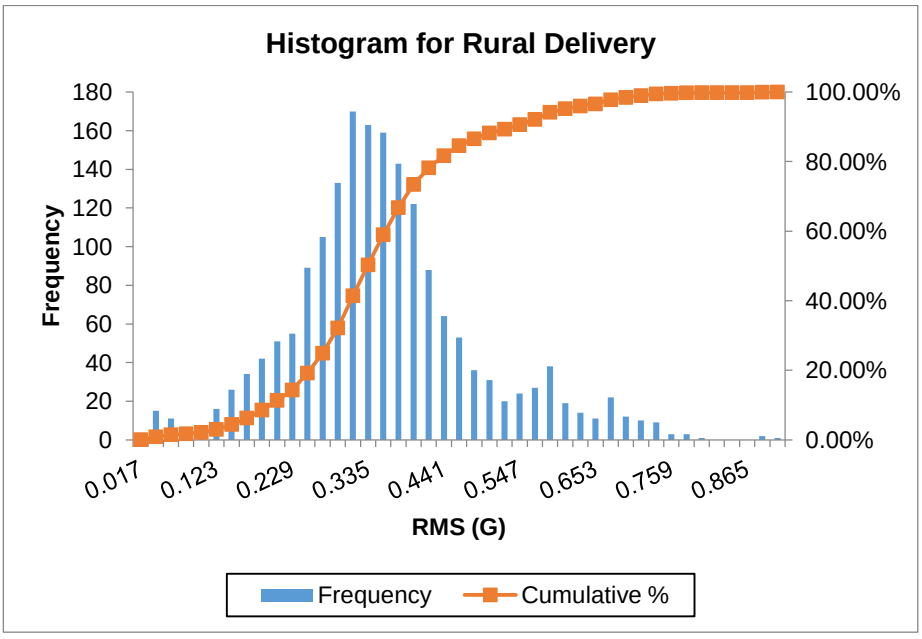

Figure 8: *Histogram for Rural Delivery – Kingsport, TN*

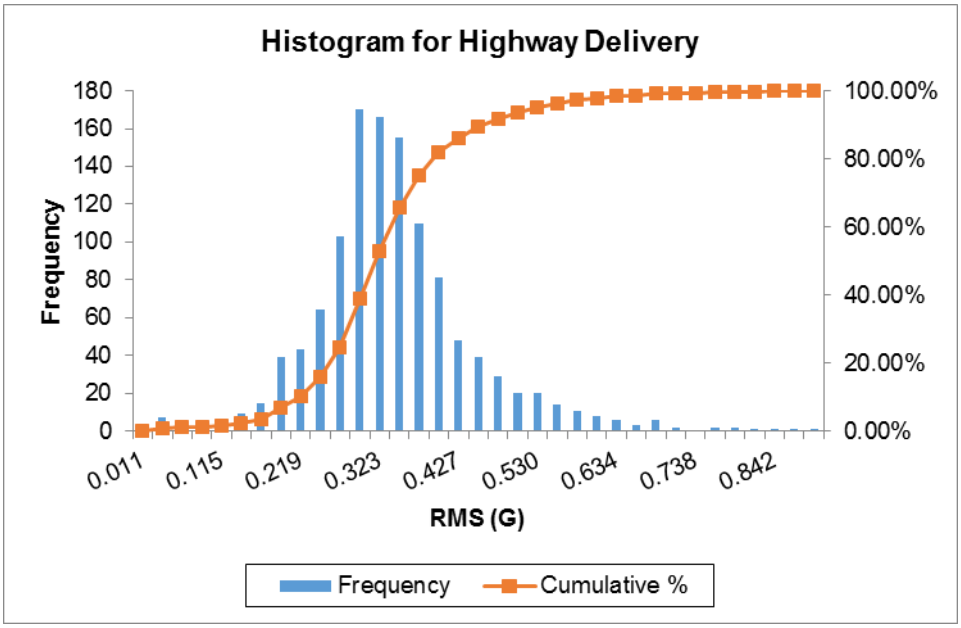

Figure 9: *Histogram for Highway Delivery – Winston-Salem, NC*

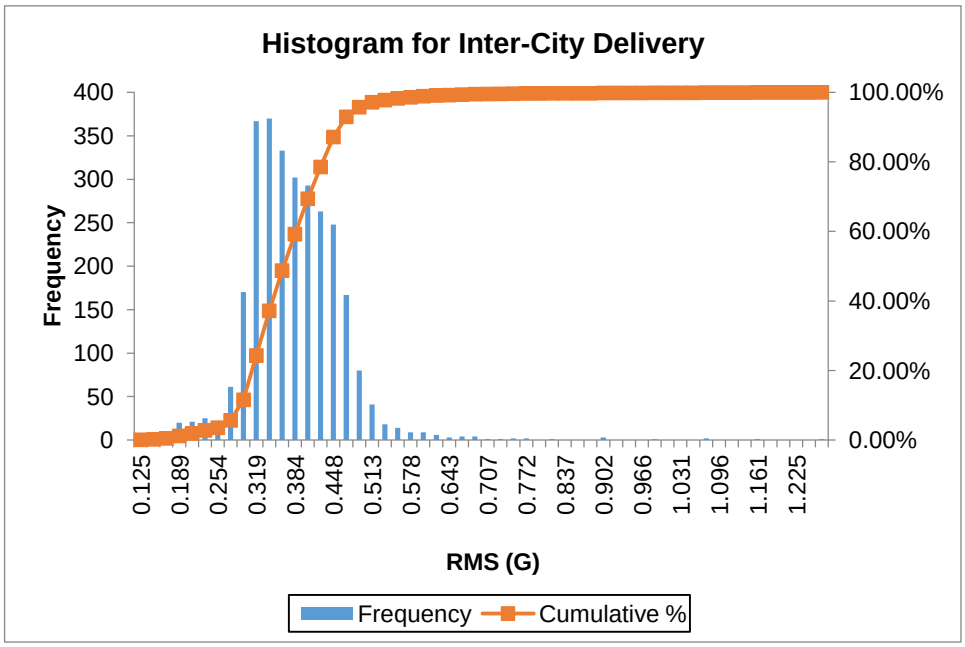

Figure 10: *Histogram for Inter-City Delivery – Atlanta, GA*

4. Conclusion

- The overall vibration intensity levels are higher in the vertical axis as compared with the lateral and longitudinal axes for all three delivery route PSD profiles.
- The inter-city delivery route produced the highest overall Grms levels, but there was not a statistical difference between the mean Grms values of the three delivery routes.
- PSD profiles produced from this study had similar ‘shaped’ curves.

- PSD profiles and Grms values can be utilized by the water bottle industry to produce a vibration test standard. In addition, the test standards can be time compressed to directly correlate to actual shipments.
- The PSD profiles which were analyzed from this research could be utilized to simulate bottled water delivery vehicles in a laboratory environment. This will enable further research in bottle and rack design, and aid in the optimization of package design and testing.

Acknowledgement

Portions of this work were supported by Eastman Chemical Company. Portions of this article were previously published and presented at the ISTA International Transport Packaging Forum™ (April 2012).

References

[1] Brandenburg, Richard & Lee, and Julian, June-Ling. 2001: *Fundamentals of Packaging Dynamics.* L.A.B. Equipment, Inc.

[2] Chonhenchob, V., Singh, S.P., Singh, J.J., Stallings, J., and Grewal, G. *Measurement and Analysis of Vehicle Vibration for Delivering Packages in Small-Sized and Medium-Sized Trucks and Automobiles.* Packaging Technology and Science. 2011. 25; 31-38.

[3] ISTA. Resource Book 2011. ISTA: East Lansing, MI, 2011,

[4] Kipp William I. *ISTA Field Data Requirements*. ISTA: East Lansing, MI, 2008.

[5] Singh, S.P., Joneson, E., Singh, J., and Grewal, G. *Dynamic Analysis of Less-Than-Truckload Shipments and Test Method to Simulate this Environment*. Packaging Technology and Science. 2008. 21; 453-466.

[6] Harris, C., Piersol, A. Harris Shock and Vibration Handbook, McGraw-Hill Professional Publishing, Dubuque, IA 52002, USA.

[7] Garcia-Romeu-Martinez, M., Singh, S.P., and Cloquell-Ballester, V. *Measurement and Analysis of Vibration Levels for Truck Transport in Spain as a Function of Payload, Suspension and Speed.* Packaging Technology and Science. 2008. 21; 439-451.

Cloud Publications
International Journal of Advanced Packaging Technology
2014, Volume 2, Issue 1, pp. 84-95, Article ID Tech-246
ISSN 2349 – 6665, doi 10.23953/cloud.ijapt.10

Research Article **Open Access**

Evaluating the Performance of Coconut Fiber and Wood Straw as Cushioning Materials to Reduce Injuries of Papaya and Mango during Transportation

Clívia Danúbia Pinho da Costa Castro[1], José de Assis Fonseca Faria[1] and Tiago Bassani Hellmeister Dantas[2]

[1]University of Campinas, Faculty of Food Engineering, Department of Food Technology, Rua Monteiro Lobato, Campinas, SP, Brazil
[2]Packaging Technology Center – CETEA/ITAL, Av. Brasil, Campinas, SP, Brazil

Correspondence should be addressed to José de Assis Fonseca Faria, assis@fea.unicamp.br

Publication Date: 30 April 2014

DOI: https://doi.org/10.23953/cloud.ijapt.10

Editor-in-Chief: **Dr. Siripong Malasri**, Christian Brothers University, Memphis, TN, USA

Abstract For the purpose to explore more ecologically sound alternatives as cushioning materials to protect fruits against injury during transport, the objective of the research was to evaluate the performance of coconut fiber and wood straw during the simulated transport of papayas and mangoes. Tests were carried out to simulate the transport of fruits in corrugated paperboard boxes in three different packaging systems: (1) with no cushioning, (2) with coconut fiber and (3) with wood straw. Physical and physiological behaviors of papaya and mango throughout transport and storage period were studied, and the rate of injuries, weight loss, skin color and respiration rate were quantified. The results showed that the coconut fiber was more efficient than wood straw in the prevention of pulp injuries, but not in prevention of abrasions on papaya surface. In mangoes, no significant differences were found between the two cushioning materials.
Keywords *Natural Fiber; Cushioning; Transport Packaging; Fruit Injuries*

1. Introduction

Economical and environmental concerns over natural resources are intensifying, which becomes evident through practices like waste utilization, alternative material development and, in some cases, substitution of fossil material by renewable material.

Of the natural fibers available, coconut fiber is becoming one of the most used in the development of environmentally friendly products, probably due to its characteristic of being an agricultural waste. In this area we find the traditional manufacturing of rope, brush and tapestry, and, more recently, automotive parts and gardening products. In general, coconut fiber presents good properties in reinforcing composite, acoustic and thermal insulation materials [1, 2, 3]. Other uses were found in absorbing material for petroleum and heavy metals [4, 5]. Some studies have mentioned the possibility of using the coconut fiber as a means of protection in packaging systems [6, 7], but the present authors found no research on the behavior of this material in the fruit industry.

Tissue paper, wood straw, molded pulp trays and expanded polyethylene nets are components commonly found in use to protect fruits and vegetables during transportation [8, 9]. Cellulosic materials have been in use for some time, but plastic materials are now more widely used, mostly for their effective performance with limited amount [10, 11]. However, ecological requirements have led to a reduction in the amount of plastic used in the manufacture of packaging [12], and more alternative materials and technologies are being studied and developed.

In the agriculture sector, horticultural products require a special attention regarding transport packaging system improvements, since in most cases such products have no primary packaging and are very susceptible to mechanical damages. Such injuries cause post-harvest loss and interfere in the classification and consumer purchase decision. Among the tropical fruits, papaya and mango present a rapid world production and commercialization [13]. These fruits are also susceptible to losses by mechanical damage, since the papaya epidermis is very thin, subjecting the microorganism penetration easily through ruptures and abrasions caused by mechanical forces during transportation [14, 15], while mango, with a thicker epidermis, develops internal damages that are not so easy to detect.

Thus, the main objective of this study is to evaluate the performance of coconut fiber as an alternative cushioning material for the transport of papaya and mango, and compare its performance to that of wood straw.

2. Materials and Methods

The raw material used for coconut fiber was the green coconut shell resulting from post-consumer disposal after coconut juice consumption. The material was obtained from kiosks and leisure facilities in Campinas, SP, and then the coconut husks were then mechanically processed into fiber. The wood straw was obtained directly from the FAPEM Ltd., a straw factory - in Campinas, SP.

A transport simulation test was conducted in order to evaluate the coconut fiber performance as a cushioning material. Two tropical fruits were selected: papaya, a fruit with a delicate structure; and the mango, that has a thicker epidermis. Papayas, variety Sunrise, and mangoes, variety Palmer, were purchased from the distributor - Campinas Central Supply Center, Campinas, SP, Brazil (CEASA Campinas). The fruits were purchased in corrugated boxes of the pre-assembled type and subsequently used in the transport simulation test. In order to standardize the experiments, fruits were selected according to the technical regulation of the Brazilian Ministry of Agriculture [16, 17]. Such requirements were used to guarantee uniformity in size, coloration and quality standard. Thus, papayas were selected from 430 to 500 grams, 15% to 25% of yellow epidermis and fruit surface with maximum limit of 5% of damage, while mangoes were selected from 400 to 500 grams, epidermis coloration from rose to red, pulp color predominantly yellow around the seed and fruit surface with maximum limit of 1% of severe damage, 5% of light damage and 5% of spots.

2.1. Transport Simulation Test

The selected fruits were physically analyzed for possible defects and packaged in three different packaging systems: (1) corrugated box with no cushioning (system 1 or control system), (2) corrugated box with coconut fiber (system 2) and (3) corrugated box with wood straw (system 3). There were fifteen fruits packed, in one layer, inside each box.

The completely randomized experimental design was used for the transport simulation, according to the 2 x 3 factorial scheme (two types of fruits and three packaging systems), adding up six treatments (Table 1 and Figure 1) with two repetitions for each treatment.

***Table 1**: Transport Simulation Test Treatments and the Respective Packaging Systems for Papaya and Mango*

Treatment	Packaging System
A	Papaya; system 1
B	Papaya; system 2
C	Papaya; system 3
D	Mango; system 1
E	Mango; system 2
F	Mango; system 3

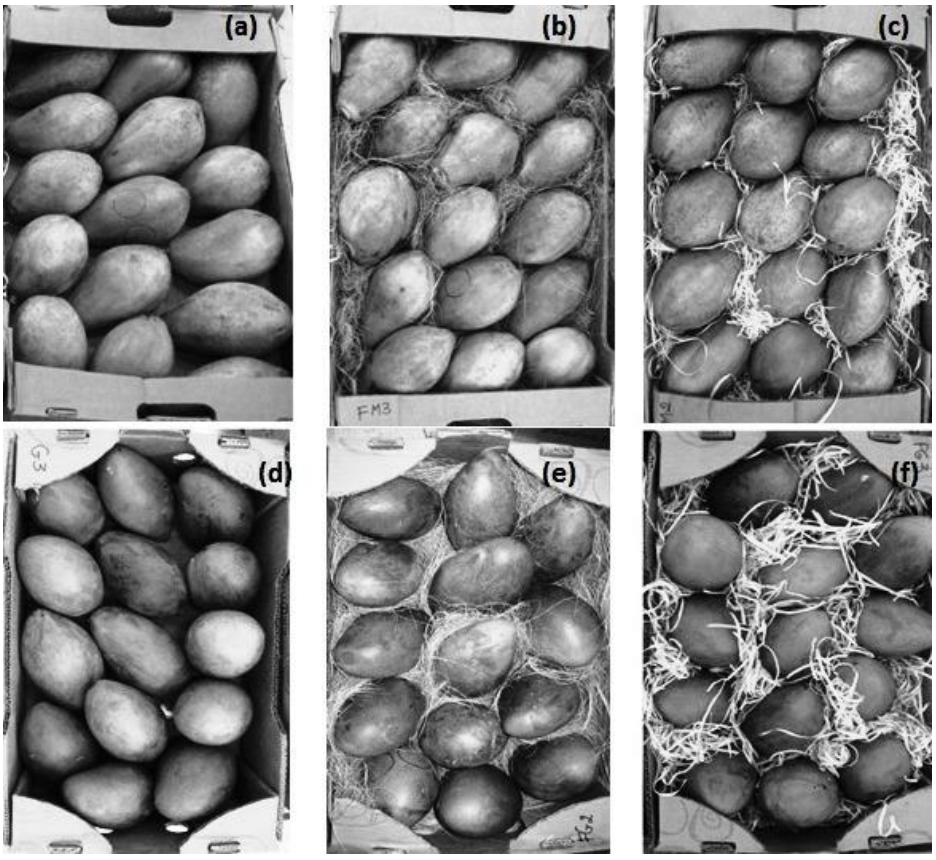

***Figure 1**: Packaging Systems Used for Papaya and Mango Transport Simulation Test: (a) Treatment A, (b) Treatment B (c) Treatment C, (d) Treatment D, (e) Treatment E and (f) Treatment F*

In order to compare the performance of coconut fiber with that of wood straw, 1.9 kg/m^2 of each material type was used inside every corrugated box. This value was based on the cushioning curves

[18] and the volumetric capacity of the boxes. For papaya, box dimensions were 0.43m x 0.27m x 0.13m and for mango were 0.54m x 0.34m x 0.13m.

The truck transport simulation test was carried out according to the ASTM D4728 (2006) procedure, using the PSD (Power Spectrum Density) for truck transportation, assurance level II with an overall g rms of 0.52, for 1 h at 23 ± 1ºC and 55 ± 1% R.H.

The fruit packages were placed directly on the MTS model 891 vibration table controlled by MTS model 407 Controller, and SignalCalc 550 Vibration Controller (Figure 2).

Figure 2: *Disposal of Packaging on a Vibration Table*

2.2. Evaluation of the Package Cushioning Systems

After the simulation test, ten papayas and ten mangoes were randomly selected from each packaging system to evaluate the performances of the cushioning materials.

The papayas were evaluated the day before simulation test (zero time) and during the six days of storage, while the mangoes were stored for eight days in a conditioned room at 24.5 ± 2ºC and 60 ± 5% R.H. During this period the fruits were classified according to their mechanical injuries, weight loss, instrumental color and respiration rate.

With respect to the injuries, the epidermis of each fruit was classified with respect to the absence or presence of *serious damages* and/or *slight damages* [16, 17]. The following were considered as *serious damages*: rupture of the epidermis covering an area greater than 5% of the fruit surface; rupture of the epidermis reaching the fruit pulp, and injury of the pulp without rupturing the epidermis; the following as *slight damages*: rupture of the epidermis covering an area less than 5% of the fruit surface.

To evaluate instrumental color, a direct reading of the external fruit surface was made using the CIELab color system. Initially green areas were selected in a random distribution such that the readings, carried out in triplicate, were analyzed from the same areas throughout the storage period.

The respiration rate was evaluated in a closed system by measuring the production of carbon dioxide by the fruit during one hour. To avoid problems due to interference caused by the accumulation of gases in the fruit tissues in this measurement; preliminary tests were carried out to

guarantee that during the storage period, the CO_2 measurement was greater than 0.2% [19]. CO_2 reading was accomplished with a MOCON Pac Check TM 650 carbon dioxide and oxygen analyzer. Respiration rate is expressed in [mg of CO_2.kg^{-1}.h^{-1}], considering dessicator volume, fruit volume and mass, and time dessicators remained closed.

The results were analyzed statistically using the analysis of variance (ANOVA), and the means of each treatment were tested for significance and compared with each other by the Tukey test ($p < 0.05$), except for the injury incidence analysis which was done by human visual inspection.

3. Results and Discussions

3.1. Papaya

For the papaya, the *appearance of injuries* was observed twenty four hours after simulation test (Figure 3). As for the comparison, none of the packaging systems evaluated was found to be effective in preventing mechanical injuries under the conditions imposed in the simulation test, since all the fruits already showed some damage on the first day of analysis.

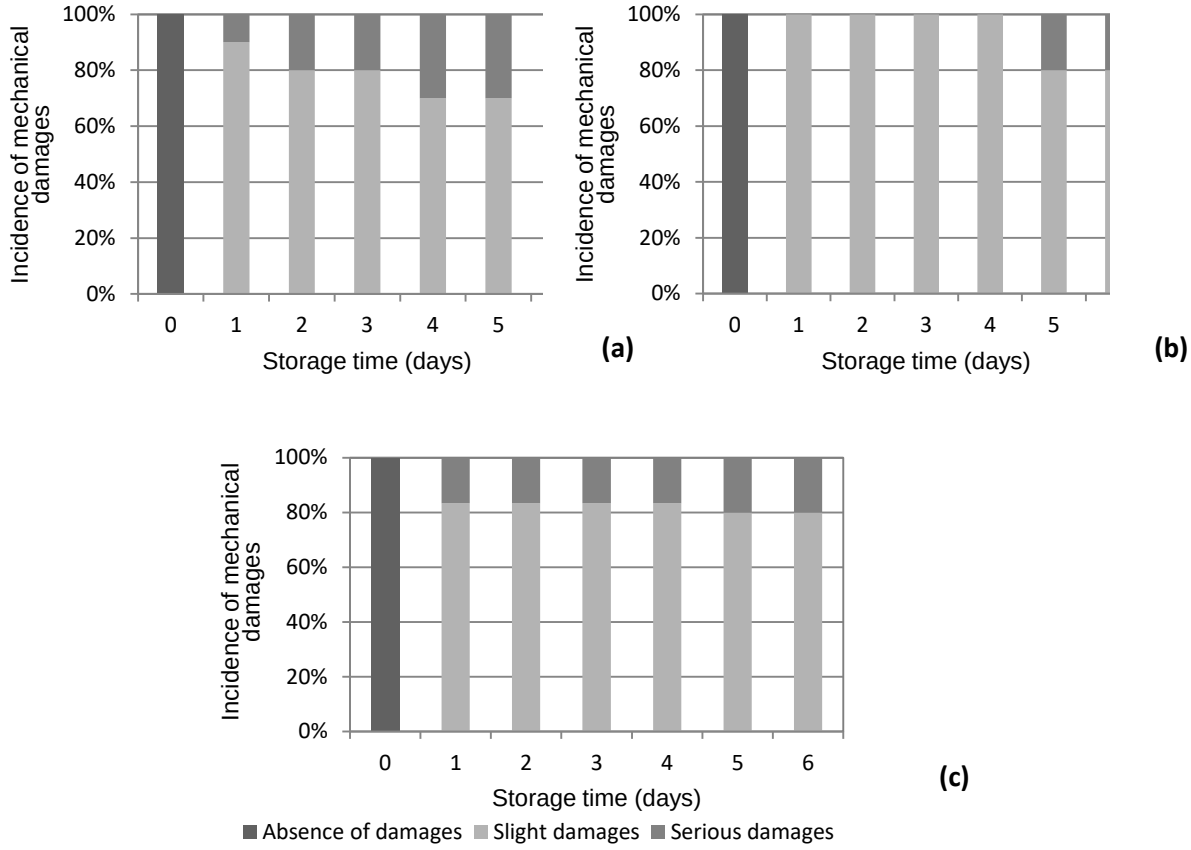

***Figure 3**: Incidence and Classification of Mechanical Damages in Papaya: a) No Cushioning; b) With Coconut Fiber; c) With Wooden Straw, Along the Storage Period*

During the evaluation of *slight damage*, epidermis injuries were observed in the system with no cushioning, highlighting the damage caused by the structure of the corrugated box. In the system with coconut fiber, the formation of deeper injuries was observed, probably due to the rotary movement of the fruit on its own axis, during the transport simulation test. In the system with wood straw, *abrasions* were found over the whole surface of contact with the straw, causing a corrugated

appearance, particularly at the end of the storage period. Abrasions were also observed in the system with coconut fiber, but the wood straw was shown to cause worse injuries on the epidermis of the fruit, as it had a thicker and coarser structure than the coconut fiber.

As for *serious damage*, the packaging system with coconut fiber was more efficient in preventing injury to the pulp than the other systems, considering that such injuries were only observed on the fifth day of storage in the papaya fruits protected by fiber. Figure 4 shows an example of serious damage to the epidermis of a papaya fruit (with no cushioning), where a well-defined dark spot can be observed located in the contact area of the fruit with the corrugated box. In this case, most of the impact energy was absorbed by the fruit and little energy was absorbed by the corrugated box, as also observed in a study with apples [20].

Figure 4: *Papaya with Serious Damage – System with No Cushioning*

Regarding *weight loss*, there was no significant difference ($p \geq 0.05$) among the treatments during the storage period. Considering that weight losses below 5% may be sufficient to reduce the value of papaya fruits [21], even papayas from the system with no cushioning remained within this loss limit up to the third day of storage. In treatment B and C such behavior was attributed to abrasions caused by the cushioning, evident from the fruit epidermis.

With respect to the *instrumental color* of the studied areas, the abrasions on the fruit surfaces were not sufficiently aggressive to cause enzymatic browning; there was an increase in luminosity during the whole storage period. In a study with Formosa papayas [22], this behavior was related to mechanical injuries, which can accelerate the metabolism of the fruit and promote a change in skin color.

As for the luminosity of the fruit skin, there was no significant difference between the treatments ($p \geq 0.05$). However, only treatments A and B remained constant during storage; results showed that fruits of treatment C had a lower luminosity at the beginning, only matching the other treatments after the fourth day of storage (Figure 5).

The results for the hue angle revealed that all systems showed a significant decrease in the values of this parameter with time (Figure 5) and there was no significant difference ($p \geq 0.05$) between them. The development of the yellow color was similar in all treatments. The average results ranged from green (111º) to yellow, tending to orange (72º).

About color intensity, the same change in chromaticity was observed for all treatments ($p \geq 0.05$). As illustrated in Figure 5, during storage, only the fruits from treatment C showed a significant difference from the second day of storage, when the hue angle defined the color of the epidermis as being between yellow and orange quadrants.

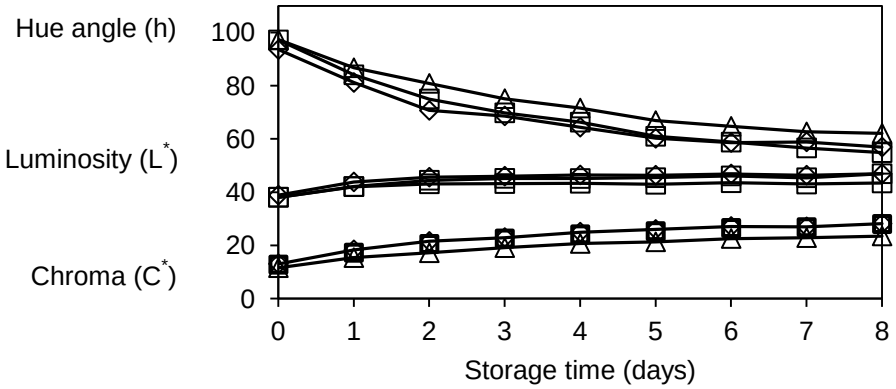

Figure 5: *Luminosity, Changes during Storage in Hue Angle and Chroma of the Epidermis of Papaya Fruits Submitted to Transport in the Following Packaging Systems: (Δ) No Cushioning, (□) with Coconut Fiber and (◊) with Wood Straw*

With respect to respiratory activity, Figure 6 shows the rate of carbon dioxide production by the papaya fruits during storage. Regarding the treatments, the wood straw system differed from the other treatments ($p < 0.05$) due to a greater production of CO_2.

Considering that an increase in *respiration rate* is generally proportional to the severity of the injuries [23], this result matches with the incidence of serious injuries observed in the pulp of papaya fruits protected by wood straw (Figure 6). Furthermore, a higher respiration rate is usually associated with a reduction in the fruit shelf life and quality loss [24].

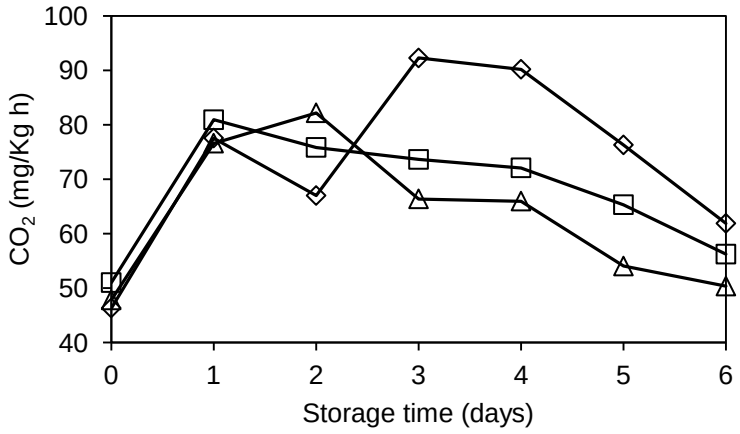

Figure 6: *Comparison of Carbon Dioxide Production during Storage by Papaya Fruits Submitted to Transport in the Following Packaging Systems: (Δ) No Cushioning, (□) with Coconut Fiber and (◊) with Wood Straw*

Thus for moderate intensity transport and distribution, coconut fiber was effective in preventing injuries from impact, but did not prevent the occurrence of injuries due to abrasion since the delicate epidermis of the Sunrise papaya requires a cushioning material made up of much thinner fibers, similar to tissue paper.

3.2. Mango

In the packaging system with coconut fiber the majority of *injuries* to mangoes were considered to be light and only found from the third day of storage (Figure 7). The cushioning systems were shown to be efficient in protecting the mangoes under the conditions imposed during the simulation test, considering that the appearance of the fruit was not compromised during storage. On the other hand, anthracnoses became evident in the epidermis of some fruits on the fifth day of storage.

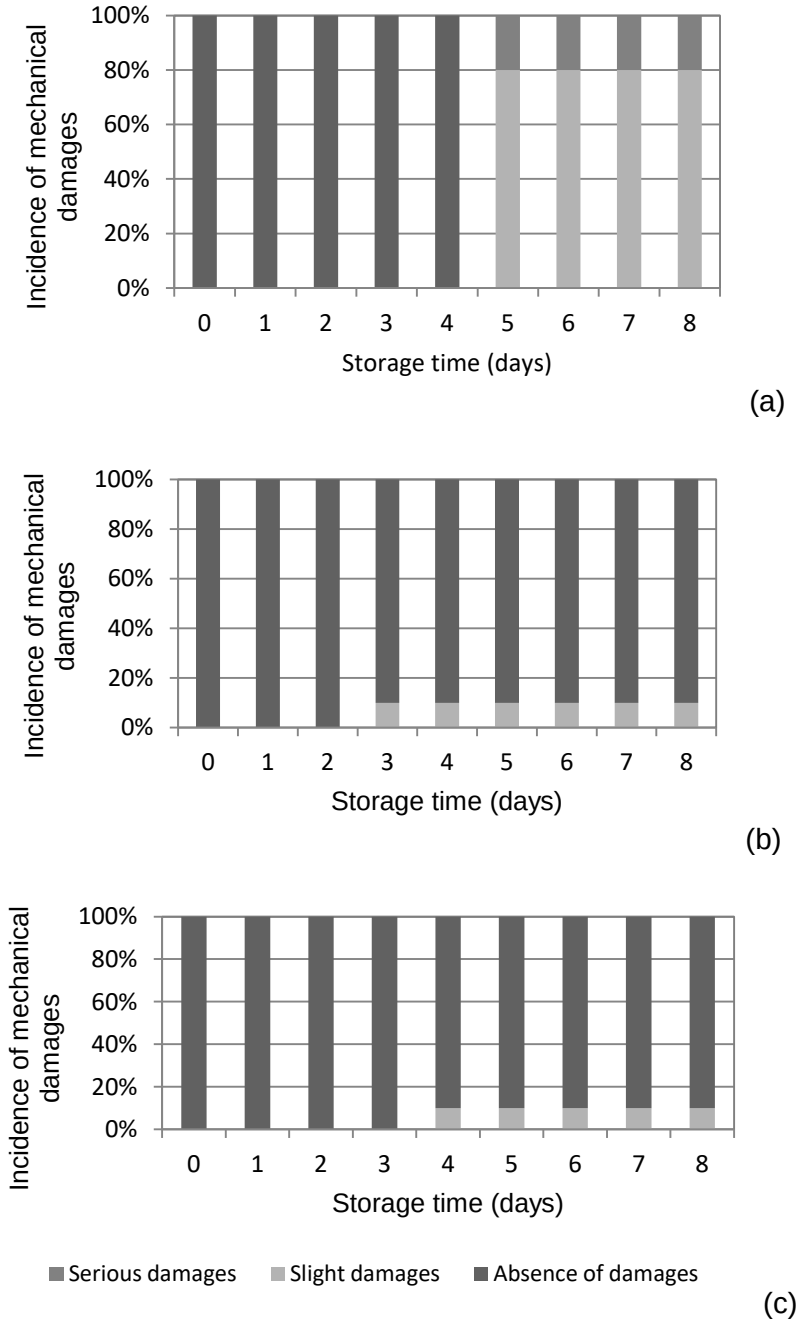

***Figure 7**: Incidence and Classification of Mechanical Damages in Mangoes: a) No Cushioning; b) with Coconut Fiber; c) with Wooden Straw, Along the Storage Period*

The results for *weight loss* during the last eight days of storage clearly showed there was no significant difference between the packaging systems evaluated ($p \geq 0.05$). The absence of *abrasions* contributed to the uniform loss in weight between the systems. Regarding weight loss, it is interesting to highlight the fact that the cellulose-based cushioning materials maintained the optimum conditions of humidity and temperature by absorbing the moisture lost from the fruit [26] thus avoiding the proliferation of fungi in high humidity environments.

The changes in skin *color* of the fruits were also highly similar between all the treatments evaluated and presented no significant difference with respect to storage time ($p \geq 0.05$). With respect to luminosity, on average the mangoes packed in fiber or straw presented a higher mean for luminosity throughout storage as compared to that of the control without cushioning, with a significant difference considering the mean values. The results for luminosity (Figure 8) are in agreement with the appearance of a greater number of injuries in the fruits without cushioning. Surface injuries of the fruits caused darkening due to enzymatic oxidation, in addition to causing metabolic changes that accelerated the senescence of the fruits [25].

The results for hue (Figure 8) showed similar behavior for all treatments, with a gradual change in yellow color towards an orange color. Such behavior is evidence of the disappearance of chlorophyll and increases in anthocyanin, total carotenoids and beta-carotene pigments in the fruit epidermis [26]. Such modifications result in greater color intensity throughout storage, principally for the color orange, as shown in the results for chroma in Figure 8.

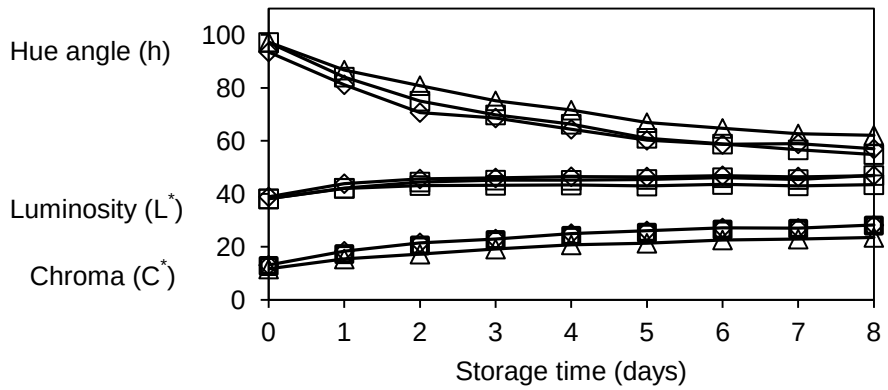

***Figure 8**: Changes in Luminosity in the Color, Values for Hue of the Skins of Mangoes, Values for Chroma Submitted to Transport in the Following Packaging Systems: (Δ) control, (□) fiber (◊) straw, During the Storage Period*

With respect to *respiratory activity*, Figure 9 shows the results for the production of carbon dioxide. The mangoes protected by coconut fiber presented similar behavior to those of the control system. On comparing the mean values obtained for the treatments, the production of CO_2 by the system with fiber was significantly lower than that for the mangoes protected by wood straw. However, with time there was no significant difference in the production of CO_2, indicating that the degree of injury caused to the mangoes was not very intense.

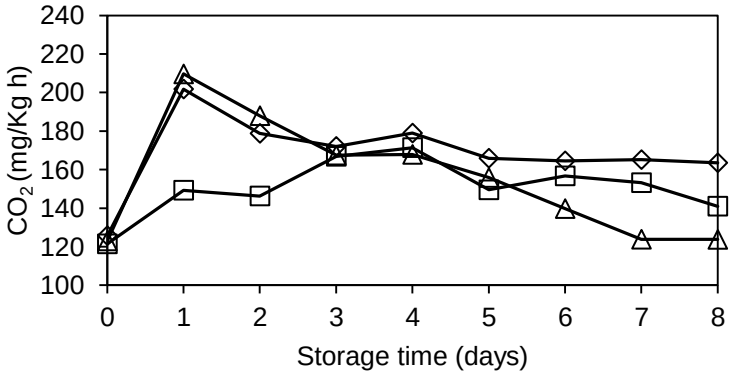

***Figure 9**: Comparison of the Production of Carbon Dioxide by Palmer Mangoes Stored at 23±2ºC as a Function of the Packaging System: (Δ) Control, (□) Fiber (◊) Straw*

4. Conclusions

Coconut fiber reduced the more serious injuries in the papaya fruits, such as those that affect the pulp, but did not prevent the incidence of abrasions during ripening. In fruits with a thicker epidermis, the number of abrasions caused by the fiber would probably be smaller.

Compared to wood straw, coconut fiber produced less damage on fruit epidermis, since the straw has a rough, more rigid surface than the fiber, and is therefore far more aggressive for delicate fruits such as the papaya. For the mangoes, it was difficult to determine bruising due to their thick epidermal, suggesting that in such case is necessary to cut the fruit open to investigate bruising effect that was not apparent from the outside of the fruit.

In general the injuries caused to the mangoes during the simulation test were not so drastic with respect to the fruit quality after transport, that is, there was little change in the natural metabolism of the fruits. No significant difference was observed between the use of coconut fiber and wood straw; both materials presented cushioning characteristics against serious injuries as compared to the treatment with no cushioning (control).

Acknowledgements

The authors are grateful to the Fundação de Amparo à Pesquisa do Estado de São Paulo (FAPESP) for their financial support and to the Brazilian Scientific Research Council (CNPq) for the research grant.

References

[1] Foluladi, M.H., Ayud, Md., and Mohd Nor, M.J. *Analysis of Coir Fiber Acoustical Characteristics*. Applied Acoustics. 2011. 72 (1) 35-42.

[2] Satyanarayana, K.G., Guimarães, J.L., and Wypych, F. *Studies on Lignocellulosic Fibers of Brazil. Part I: Source, Production, Morphology, Properties and Applications.* Composites Part A: Applied Science and Manufacturing. 2007. 38 (7) 1694-1709.

[3] Silva, G.G., Souza, D.A., De, Machado, J.C., and Hourston, D.J. *Mechanical and Thermal Characterization of Native Brazilian Coir Fiber*. Journal of Applied Polymer Science. 2000. 76 (7) 1197-1206.

[4] Annunciado, T.R., Sydenstricker, T.H.D., and Amico, S.C. *Experimental Investigation of Various Vegetable Fibers as Sorbent Materials for Oil Spills*. Marine Pollution Bulletin. 2005. 50 (11) 1340-1346.

[5] Igwe, J.C., Abia, A.A., and Ibed, C.A. *Adsorption Kinetics and Intraparticulate Diffusivities of Hg, As and Pb ions on Unmodified and Thiolated Coconut Fiber*. International Journal of Environment Science Technology. 2008. 5 (1) 83-92.

[6] Grimwood, B.E., 1975: *Coconut Palm Products: Their Processing in Developing Countries*. Food and Agriculture Organization of the United Nations, Roma.

[7] Osborn, D.B., 1967: *Package Cushioning Systems*. Packaging Materials and Containers, Blackie e Son Limited, London.

[8] Chonhenchob, V., and Singh, P. *Packaging Performance Comparison for Distribution and Export of Papaya Fruit*. Packaging Technology and Science. 2005. 18 (3) 125-131.

[9] Luengo, R. de F.A., and Calbo, A.G., 2006: Embalagens para comercialização de hortaliças e frutas. Circular Tecnica, Brasília, DF Dezembro.

[10] Mckinlay, A.H., 2004: *Cushioning Systems: Interior Packaging for Shock and Vibration Protection*. Transport Packaging, New York. 109-123.

[11] Ramsland, T., 1989: *Cushioning Materials*. Handbook on Procurement of Packaging, PRODEC, Finland.

[12] Gonzalez, P.M., and Zepka M.M., 2008: Embalagens e materiais de acolchoamento e o meio ambiente. Portal de Embalagens.

[13] FAO (Food and Agriculture Organization of the United Nations), 2010: Fibre. http://faostat.fao.org.

[14] Bollen, A.F., Nguyen, H.X., and Dela Rue, B.T. *Comparison of Methods for Estimating the Bruise Volume of Apples*. Journal of Agricultural Engineering Research. 1999. 74 (4) 325-330.

[15] Timm, E.J., and Brown, G.K. *Impacts Recorded on Avocado, Papaya, and Pineapple Packing Lines*. Applied Engineering in Agriculture. 1991. 7; 418-422.

[16] Brasil, Portaria nº249, de 29 de julho de 2009. Anexos do regulamento técnico do mamão.

[17] Brasil, Portaria nº689, de 21 de novembro de 2002. Regulamento técnico de identidade e de qualidade da manga.

[18] Castro, C.D.P.C., Faria J.A.F., and Dantas, T.B.H. *Testing the Use of Coconut Fiber as a Cushioning Material for Transport Packaging*. Materials Science and Applications. 2012. 3 (3) 151-156.

[19] Kader, A.A., and Saltveit, M.E., 2003: *Respiration and Gás Exchance*. Postharvest Physiology and Pathology of Vegetables, Marcel Dekker, New York.

[20] Jarimopas, B., Singh, S.P., and Sayasoonthorn, S. *Test Method to Evaluate Bruising During Impacts to Apples and Compare Cushioning Materials*. Journal of Testing and Evaluation. 2007. 35. 1-6.

[21] Cenci, S.A., 2002: *Procedimentos pós-colheita. Mamão: pós-colheita. Brasília*. Embrapa Informação Tecnológica.

[22] Santos, C.E.M., Couto D'Araújo, F.A., Salomão, L.C.C., Cecon, P.R., Júnior, A.W., and Bruckner, C.H. *Comportamento pós-colheita de mamões Formosa 'Tainung 01' acondicionados em diferentes embalagens para o transporte*. Revista Brasileira de Fruticultura. 2008. 30. 315-321.

[23] Kader, A.A., 1987: *Respiration and Gas Exchange of Vegetables*. Postharvest Physiology of Vegetables, Marcel Dekker, New York.

[24] Phan, C.T., 1975: *Respiration and Respiratory Climacteric*. Postharvest Physiology, Handling and Utilization of Tropical and Subtropical Fruits and Vegetables.

[25] Mohsenin, N.N., 1986: *Physical Properties of Plant and Animal Materials: Structure, Physical Characteristics and Mechanical Properties*. Gordon and Breach, New York.

[26] Lakshminarayana, S., 1980: *Mango.* Tropical and Subtropical Fruits: Composition, Properties and Uses. AVI Publishing, Westport.

Cloud Publications
International Journal of Advanced Packaging Technology
2014, Volume 2, Issue 1, pp. 96-104, Article ID Tech-277
ISSN 2349 – 6665, doi 10.23953/cloud.ijapt.11

Research Article **Open Access**

Softwood Pallet Stringer Temperature Estimation

Ali Pourhashemi and Siripong Malasri

Healthcare Packaging Consortium, Christian Brothers University, 650 East Parkway South, Memphis, TN, USA

Correspondence should be addressed to Ali Pourhashemi, apourhas@cbu.edu

Publication Date: 18 June 2014

DOI: https://doi.org/10.23953/cloud.ijapt.11

Abstract Monitoring temperature inside a pallet specimen during a test could be challenging. In this study, two methods were used to estimate temperature in a softwood pallet stringer at the time of testing based on the initial temperature of when it was removed from a temperature chamber and the duration of when it was removed from a chamber until the time it was tested. Five cooling down and three warming up temperature profiles were collected using thermocouples. In the first method, an artificial neural network was developed based on the collected data. In the second method, a mathematical model was suggested based on heat transfer principles. Collected data was used to validate the model. Both methods yield satisfactory results. The heat transfer model allows temperature estimation for specimens with different thickness and species, while the neural network is more precise but limited to the specimen used. Both methods allow other researchers to estimate the temperature without having to collect temperature data.
Keywords *Wooden Pallets; Temperature Estimation; Heat Transfer; Artificial Neural Network*

1. Introduction

In a previous study of the temperature effect on static and impact properties of new softwood pallets [1], static compression tests, drop tests, and incline impact tests were performed at different temperatures ranging from $35^{\circ}F$ to $160^{\circ}F$. Tests could ideally be performed in a temperature-controlled chamber. However, typically these chambers are small. Having large test equipment within a custom-built chamber could be expensive and would risk equipment damages due to extreme temperature. Thus, in this previous study, thermocouples were used to monitor temperatures from the time a specimen was removed from a temperature chamber until it was stabilized at a normal room temperature of $73^{o}F$. This stabilizing temperature is considered as the

normal test environment by ISTA test protocols, including ISTA Procedure 3A [2]. Equation 1 was developed and used to estimate the temperature inside a specimen at the time of testing:

$$T = \begin{cases} (1.8E-06)t^4 - 0.0006t^3 + 0.0701t^2 - 3.6542t + 160 & \text{for cooling down} \\ (1E-07)t^5 - (3E-05)t^4 + 0.003t^3 - 0.135t^2 + 3.1365t + 32.736 & \text{for warming up} \end{cases} \quad \text{... Eqn. 1}$$

Where t = time (minutes) and T = temperature (^{o}F). These equations are specific to Yellow Pine stringers, which are widely used in the Southern part of the United States. It was also discussed in the same previous study mentioned above, that the range of temperature in developing a temperature profile has significant effect on a temperature prediction.

This article presents two different methods in estimating temperature based on initial temperature in which a specimen is preconditioned and the time elapsed from the instant it is removed from a temperature chamber to the time of testing. In the first method, an artificial neural network was trained to recognize the temperature data collected from five cooling down and three warming up curves. In the second method, an equation based on heat transfer principles was developed and validated with the collected data.

2. Materials and Methods

2.1. Data Collection

A pallet stringer specimen was placed in a temperature chamber set at different temperatures, i.e., 35 $^{\circ}F$, 45 $^{\circ}F$, 55 $^{\circ}F$, 100 $^{\circ}F$, 120 $^{\circ}F$, 140 $^{\circ}F$, 160 $^{\circ}F$, and 180 $^{\circ}F$ until the temperature at the center of the specimen stabilized. Then it was removed from the chamber and left at room temperature of about 73 $^{\circ}F$. A thermocouple was inserted into the sample. Data was collected at 1-minute intervals through a data acquisition system until it was stabilized at the room temperature. Figure 1 shows the temperature chamber (left) used in the study, a specimen with thermocouples (middle) along with data acquisition system (right). It should be noted that the thermocouple entry points into the specimen were covered with foam (not shown in Figure 1) to avoid heat leakage.

Figure 1: *Data Collection Equipment and Instrumentation [1]*

2.2. Artificial Neural Network

Each cooling down or warming up curve was plotted and fitted with a trend line. The trend line equation was used to generate data for training and validating a neural network. 80% of the generated data was used for training while the remaining 20% was used for validation. A feed-forward, fully-connected back propagation neural network was used with two input cells, sixteen hidden cells, and one output cell, as shown in Figure 2. A bias cell (cell with input of 1) was added to each hidden and output cell. The sigmoid function, $y = \frac{1}{1+e^{-x}}$, was used to generate an output of each hidden and output cell, where x is a weighted sum (sum of the product of a connection weight and the input value going through it) and y is the output of that particular cell.

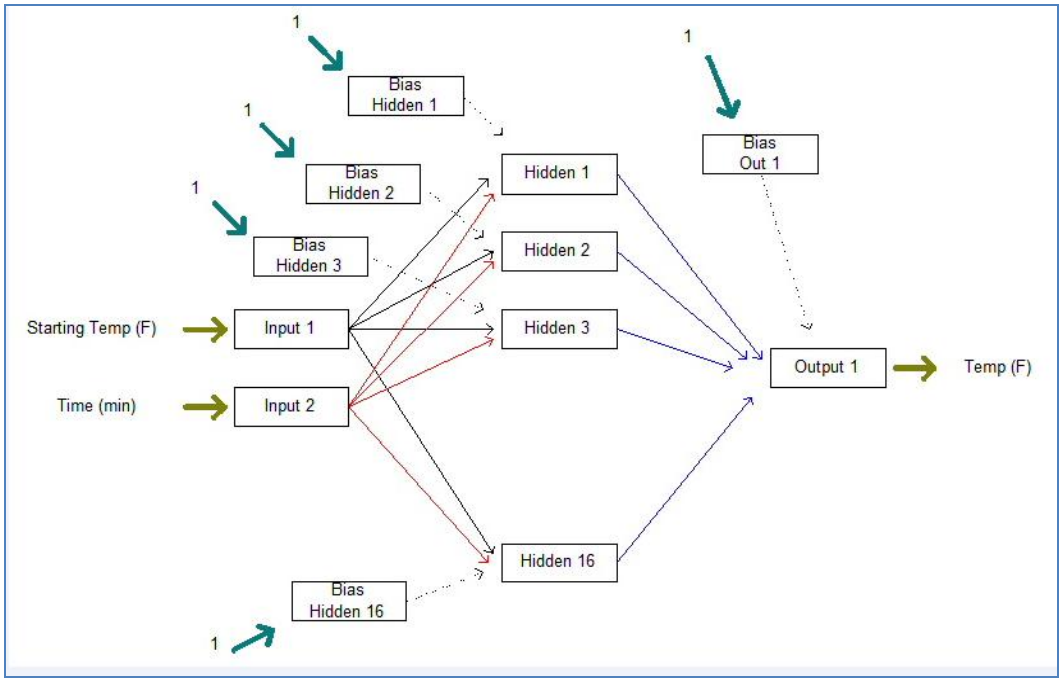

Figure 2: *Neural Network Configuration*

During a training session, errors of predicted values and desired values were minimized through an iterative process of forward and backward passes. Once the errors were at an acceptable level, the network was used to predict the output using only the forward pass for a given set of input figures.

2.3. Heat Transfer Model

Equation 2 is a general heat conduction equation for heat transfer in three dimensions [3].

$$\rho C_p \frac{\partial T}{\partial t} = k\left(\frac{\partial^2 T}{\partial x^2} + \frac{\partial^2 T}{\partial y^2} + \frac{\partial^2 T}{\partial z^2}\right) \qquad \text{… Eqn. 2}$$

Figure 3 shows a sketch of heat conduction in a slab which represents a stringer sample. The specimen thickness (*D*) and depth (*w*) are fixed. The length (*L*) of a specimen of 10 inches was chosen. Since the width is the thinnest part, heat dissipates primarily along this dimension. Thus, this is a one-dimensional flow problem.

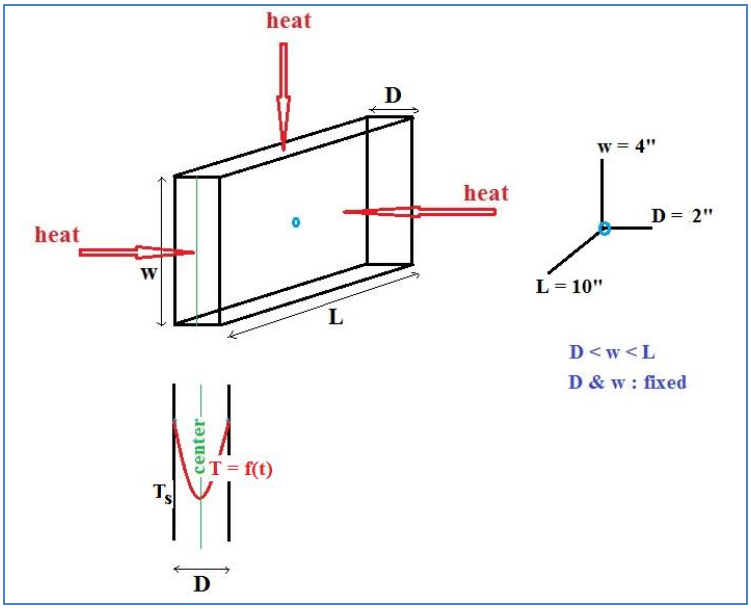

Figure 3: *Heat Conduction in a Slab*

Heat transfer in pallet stringers primarily occurs in one direction, along the thickness which is the thinnest part. Thus, Equation 2 can be reduced to:

$$\rho C_p \frac{\partial T}{\partial t} = k\left(\frac{\partial^2 T}{\partial x^2}\right) \qquad \text{… Eqn. 3}$$

Where ρ = density (kg/m^3), C_p = heat capacity (J/kg·K), k = thermal conductivity (W/m·K), T = temperature ($^\circ F$), and t = time (minutes).

Density (ρ), heat capacity (C_p), and thermal conductivity (k) were assumed to be constant during the heat transfer process due to a small temperature range. The surface temperature (T_s), which is the room temperature during the warming up or cooling down was also constant, while at the center of the specimen ($x = 0$) the heat transfer rate, $\frac{dT}{dx}$ was zero. The final one-dimensional, unsteady-state heat conduction model was suggested according to [3]:

$$T(x,t) := T_s + \frac{2(T_0 - T_s)}{\pi}\sum_{n=1}^{200}\left[\left(\sin(x\cdot\beta(n))\right)\cdot e^{-\left[\alpha t(\beta(n))^2\right]}\left[\frac{1-(-1)^n}{n}\right]\right] \qquad \text{... Eqn. 4}$$

Where L = thickness of the specimen (inches), x = local distance from the center (inches), T = transient temperature ($^\circ F$), T_0 = initial temperature ($^\circ F$), T_s = final room or the surface temperature ($^\circ F$), t = time (minutes), α = thermal diffusivity (m/s^2) = $\frac{k}{\rho}C_p$, β(n) = Eigen value (m^{-1}) = $n\frac{\pi}{L}$ and n =1, 2, 3…..

3. Results and Discussion

3.1. TempNet: A Neural Network for Temperature Estimation

Trend line equations, shown in Table 1, were generated from the collected data. It should be noted that these trend lines change the starting temperature somewhat, such as 56 $^{\circ}F$ instead of 55 $^{\circ}F$ and 165 $^{\circ}F$ instead of 160 $^{\circ}F$. In these equations, x is time (minutes) and y is temperature ($^{\circ}F$).

Table 1: *Trend Line Equations*

Trend Line Equations	R^2
$y_{188} = -0.0002x^3+0.0507x^2-3.892x+187.75$	0.9983
$y_{165} = -0.0002x^3+0.046x^2-3.3304x+165.18$	0.9979
$y_{142} = -0.0001x^3+0.0282x^2-2.3376x+142.41$	0.9977
$y_{123} = -9E-05x^3+0.0214x^2-1.6869x+123.34$	0.9965
$y_{103} = -5E-05x^3+0.0116x^2-0.9459x+102.9$	0.9922
$y_{56} = 4E-05x^3-0.0086x^2+0.6485x+55.627$	0.9837
$y_{45} = 5E-05x^3-0.0114x^2+0.9178x+45.417$	0.9916
$y_{35} = 7E-05x^3-0.0157x^2+1.1888x+35.128$	0.9935

A total of 248 examples generated from these trend lines (shown in Figure 4 and Table 2) are used in the neural network development. Out of the 248 examples, 199 were used in training the network (seen data) and 49 were used in validating the network (unseen data).

NeuroShell 2 [4] was used to train the neural network using training parameters shown in Figure 5. The performance of the network in terms of error percentage of the desired output is summarized in Table 3. The software also generated a generic source code as shown in Appendix A. A spreadsheet, TempNet [5], was then developed following the logic given in this generic source code as shown in Figure 6. In addition, two starting temperatures not part of the collected data, represented by the two solid-line graphs in Figure 7, were used to test the network ability to generalize, i.e., interpolation between graphs from collected data. It is clear that the network has ability to recognize the patterns of how temperature changes with time.

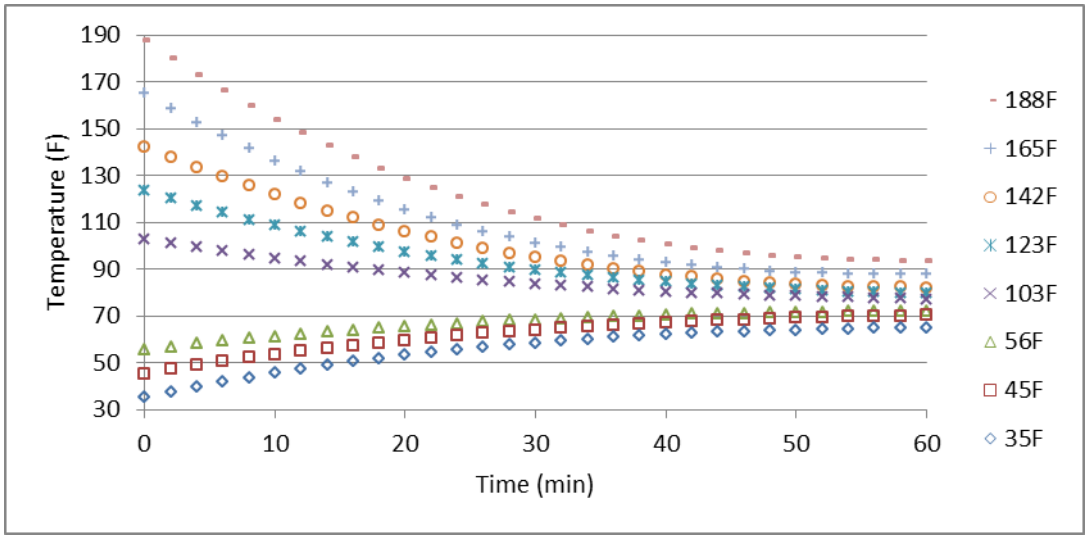

Figure 4: *Data for Network Development*

Table 2: *Training Data (T) and Validation Data (V)*

START	TIME	TEMP	MARK	NOTES
35	0	35	T	T = Training (Seen Data)
35	2	37	T	
35	4	40	T	
35	6	42	T	
35	8	44	V	V = Validation (Unseen Data)
35	10	46	T	
35	12	47	T	
35	14	49	T	
188	50	95	T	
188	52	94	T	
188	54	94	V	
188	56	94	T	
188	58	94	T	
188	60	94	T	

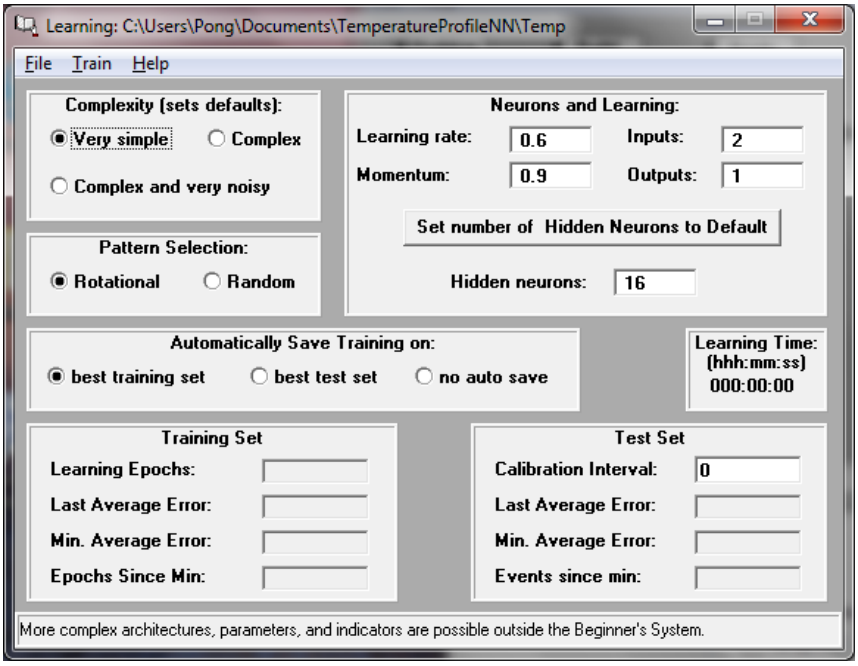

Figure 5: *Network Training Parameters*

Table 3: *Network Performance*

Group	Seen Data (T)	Unseen Data (V)	All Data (T + V)
Number of Examples	199	49	248
Minimum Error (%)	0.01	0.04	0.01
Maximum Error (%)	5.76	3.89	5.76
Average Error (%)	1.23	1.15	1.21

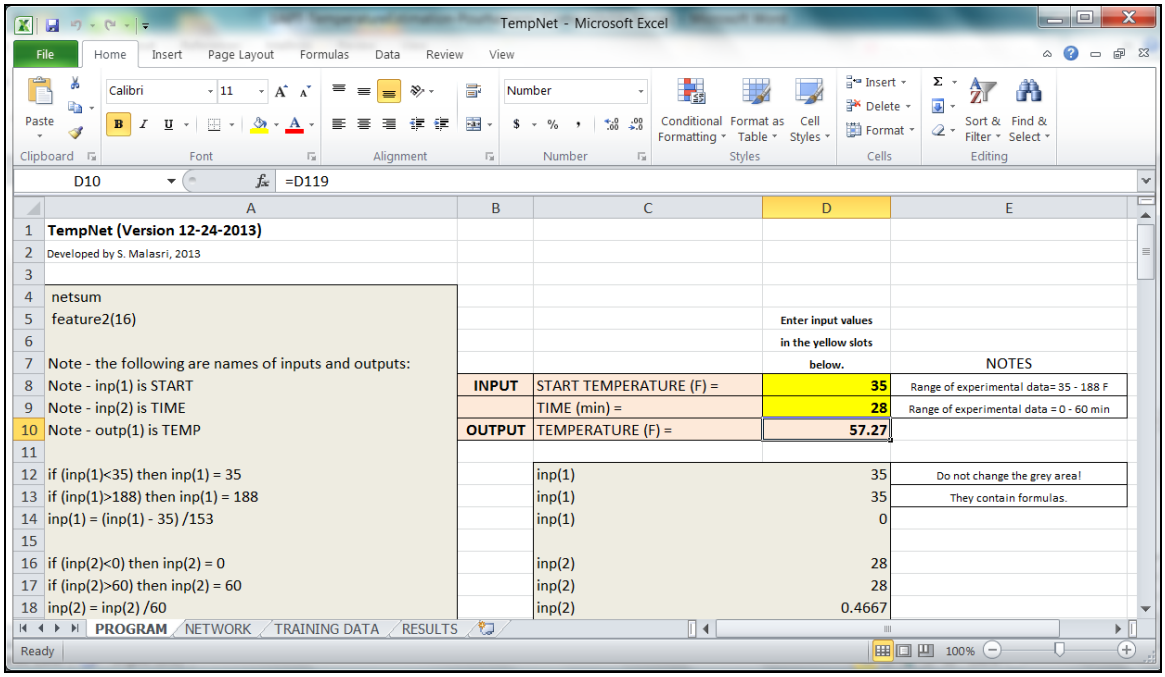

Figure 6: *TempNet Spreadsheet [5]*

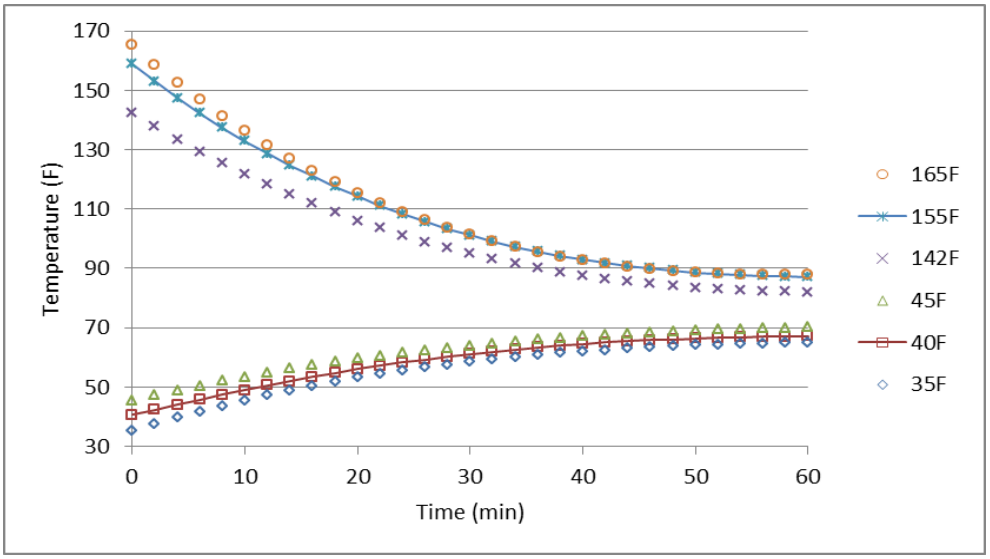

Figure 7: *Network Ability to Interpolate Between Know Values*

3.2. Heat Transfer Model

The heat transfer model presented earlier was used to estimate temperature. Comparison was made with actual collected data in Figure 8. Using the physical properties [6], the model-predicted temperature profiles were compared with the experimental data for various temperature settings. The equation was verified for various initial temperature settings and only one setting (T_o= 180 °F) is presented in this paper. Overall, the model-predicated temperatures have shown a close agreement with the experimental data for all surface temperature settings (T_s = room temperature) and depths. The over prediction of temperature in the early transient period was due to assumption of a high constant surface temperature in the equation. For example, Figure 9 compares the theoretical T_s with the experimental data as it reaches steady state. The experimental T_s is not constant during the

transient period, but it recovers gradually and it reaches to about 70% of the final temperature within 15 minutes. Although the difference between the experimental and the theoretical T_s seems noticeable in Figure 9, the predicted temperatures of inner layers are within acceptable range as shown by a 10% error bar in Figure 8. One may also argue that assumption of a natural convective boundary condition rather than constant T_s at the surface may improve the accuracy of the temperature prediction of the inner layers, but this requires detailed calculation of the heat transfer coefficient (i.e., f (Gr no. and Pr. no)) at various surrounding conditions which is not required for this work and its practical application. Therefore, assumption of a constant surface temperature provides sufficient ability to predict the temperature data with about 90% accuracy in most cases. (Legends: Gr no: Grashof number, Pr no: Prandtl number)

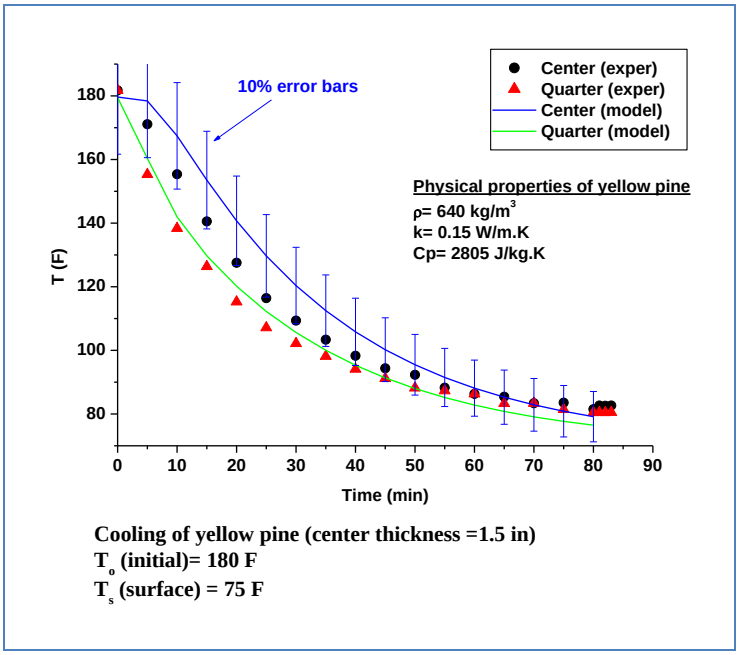

Figure 8: *Comparison of Temperature Profiles (Experimental vs. Model)*

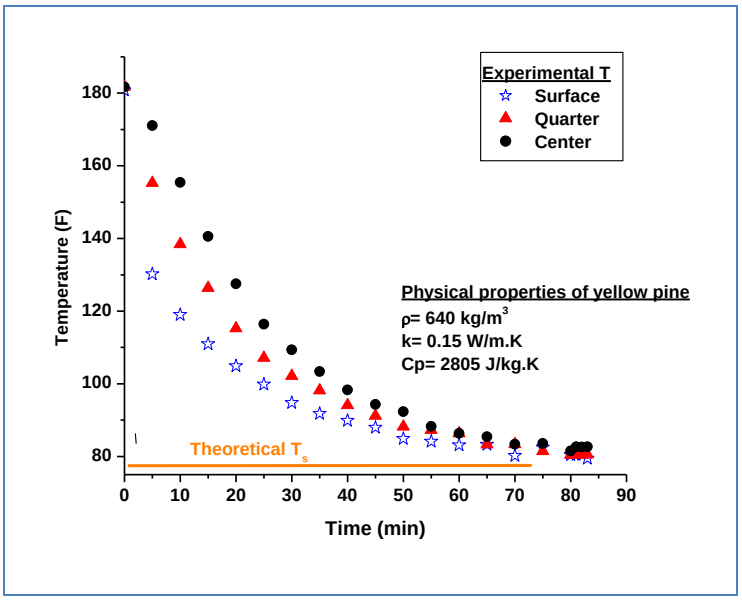

Figure 9: *Comparison of Experimental and Theoretical Surface Temperatures*

4. Conclusion

Both methods give effective predictions of the temperature inside the specimen. The neural network model is quite accurate since it was developed based on the collected data. However, it is limited to the Yellow Pine pallet stringers with a 2-inch thickness. The heat transfer model is less accurate but can be applied to different species of wood and thickness. The two models presented will eliminate the time-consuming data collections and manipulation for determination of pallet temperature.

References

[1] Malasri, S., Pourhashemi, A., Brown, R.W., Harvey, M., Moats, R., Godwin, K., Aung, P., and Laney, J. *Effect of Temperature on Static and Impact Properties of New Softwood Pallets*, International Journal of Advanced Packaging Technology. 2013. 1 (1) 30-39.

[2] ISTA Procedure 3A, 2008: *Packaged-Products for Parcel Delivery System Shipment 70 kg (150 lb) or Less*. International Safe Transit Association, East Lansing, MI.

[3] Hohn, D.W., Ὂzisik, M.N., 2012: Heat Conduction. John Wiley & Sons Inc.

[4] Ward Systems Group, Inc. *NeuroShell 2*. http://www.wardsystems.com/neuroshell2.asp (As of December 31, 2013)

[5] Malasri, S. *Packaging e-materials*. http://facstaff.cbu.edu/pong/e-Materials.html (As of May 4, 2014)

[6] Incropera, F.P., and DeWitt, D.P., 2002: *Heat and Mass Transfer*. 5th Ed. John Wiley & Sons.

Cloud Publications
International Journal of Advanced Packaging Technology
2014, Volume 2, Issue 1, pp. 105-111, Article ID Tech-282
ISSN 2349 – 6665, doi 10.23953/cloud.ijapt.12

Research Article **Open Access**

Analysis of In-Flight Vibration of a Single-Engine Propeller Aircraft

Kyle Dunno

Department of Food, Nutrition, and Packaging Sciences, Clemson University, Clemson, South Carolina, U.S

Correspondence should be addressed to Kyle Dunno, kdunno@clemson.edu

Publication Date: 19 June 2014

DOI: https://doi.org/10.23953/cloud.ijapt.12

Abstract Shipping companies are employing the use of all modes of transportation, including air transport, to decrease the costs and amount of time associated with delivering goods on time to the end user. Packaged products therefore are introduced to a variety of hazards while being transported. One way to evaluate a packaged product's ability to withstand these hazards is to perform laboratory simulated tests designed to replicate and reproduce field data results. Current industry standards employed for evaluating and testing shipments by aircraft are potentially too severe and can result in over testing and produce false results. A single-engine propeller aircraft was instrumented with a field data recorder and vibration data was collected and analyzed. By using the internal pressure sensor of the field data recorder, the vibration data could be separated based on ground and in-flight vibration. The results of this project showed the in-flight vibration intensity is much lower than what current industry standards have published. The resulting power spectral density (PSD) profile can be used to evaluate packages traveling in a small parcel environment where a single-engine propeller plane will be employed.
Keywords *Aircraft Vibration; Vibration Testing; Air Transport; PSD Profiles*

1. Introduction

Over the past twenty years there has been a steady rise in products being purchased through e-commerce and dotcom businesses. Consumers purchasing goods through these sectors often have the ability to select next day or overnight delivery of the goods with a guaranteed delivery time. One of the common modes of transportation for these types of delivery systems is via aircraft.

There are other reasons for the increasing importance of air transportation. For example, in recent years the use of logistics to manage a supply chain has increased due to companies needing to reduce the costs of tied-up capital investments [1]. The logistical way of thinking becomes more and

more common, where companies aim to reduce the costs of tied-up capital. The time factor has become more important as faster transport combined with efficient material flow means excess supplies are reduced along with storage costs. Additionally, the increased competition demands manufacturers to be alert to market changes more quickly – which means being able to forecast the flow of goods properly [2].

The rise in air transportation has led to the need to understand and properly characterize this distribution channel. Packages are transported via multiple distribution channels to reach their specified destinations. Throughout the various distribution channels, the packaged products are subjected to three major categories of dynamic hazards: shock, vibration, and compression. While shock and compression hazards cannot be overlooked when designing packages or packaging materials, the basis of this research focuses on vibration, specifically aircraft vibration.

The intensity of vibration experienced by a packaged product depends on the type of transportation used. Different modes of transport will produce different vibration inputs to the packaged product system. The vibration environment on cargo aircraft is broadly classified into two sources; internal and external. The excitation frequencies are highly dependent on the type of aircraft (turbojet, turboprop, reciprocating engine, or helicopter); while the amplitudes depend more on the flight mode (takeoff, climb, cruise, and landing) [3]. The internal sources of vibration are the aircraft's engine and the means of transferring the power into thrust. The external sources of vibration are air turbulence, intermittent air pockets, and weather patterns.

Multiple types of aircraft are used to transport materials and packages throughout the world. Collectively, these types of aircraft can be summarized into two main categories – jet engine and turbo propeller (feeder aircraft). Some jet engine aircraft commonly used by the United Parcel Services (UPS) in transporting materials and packages are Boeing 757-200 Freighter and the DC8-70 Freighter [4]. While these larger aircrafts can transport thousands to millions of packages to major metropolitan cities, if the packaged products destination is not immediately served by a major airport or is remotely located, it may be introduced into a feeder aircraft network in order to aid in delivering the package on time [5].

The objective of this research is to capture and characterize in-flight aircraft vibration occurring during the shipment of packaged products to better understand this distribution channel. Air transportation is a highly used mode of transportation today due to the ability to conduct overnight and next day shipments. With the advent of more powerful and versatile data recorders, such as Lansmont's SAVER™ 9x30 (Lansmont Corp., Monterey, CA), this study aims to better characterize in-flight vibration data for a single-engine propeller aircraft. Utilizing the data recorder's internal pressure sensor, vibration data can be separated into ground data and air data, enabling the creation of separate power spectral density (PSD) profiles. These separate vibration profiles enable future research to be conducted in the air transport environment and aid in the optimization of package design.

2. Materials and Methods

2.1. Published Air Vibration PSD Profiles

Currently, two published air vibration test profiles are available for evaluating packaged products: one within the ASTM D 4169–09 "Standard Practice for Performance Testing of Shipping Containers" and the other is located in ISTA 4AB [6, 7]. Additionally, two profiles were developed from studies conducted by Amgen and Lansmont Corporation using an instrumented unit load device (ULD) inside the aircraft and at Clemson University using an instrumented Rockwell Twin

Engine aircraft [8, 9]. Figure 1 depicts the following four PSD profiles: ASTM D 4169–09 Air Assurance Level II, ISTA 4AB, the Amgen study, and the Rockwell study. All of the profiles depicted are different from each other, but there are similarities between the ISTA 4AB, Amgen, and Rockwell profiles when comparing the frequency domain signature. With this result, it was determined that more research of the air transportation environment was needed to better characterize each aircraft's profile.

Both the ISTA 4AB and Amgen studies were conducted with an instrumented package placed inside of the cargo area of the aircraft. The package in both instances was a ULD. Both studies measured the container's response to the vehicle vibration, not the input itself from the vehicle. Current data collection techniques for obtaining over-the-road vibration data for a truck require the attachment of a recorder to the floor of the vehicle, and the data collected from those recorders is used to drive a vibration table simulation [10]. The Rockwell Twin Engine turbo propeller study and the current Cessna 172 aircraft study differs from other published studies by measuring vibration input into the cargo area of a turbo propeller aircraft versus measuring a package's response to such vibration.

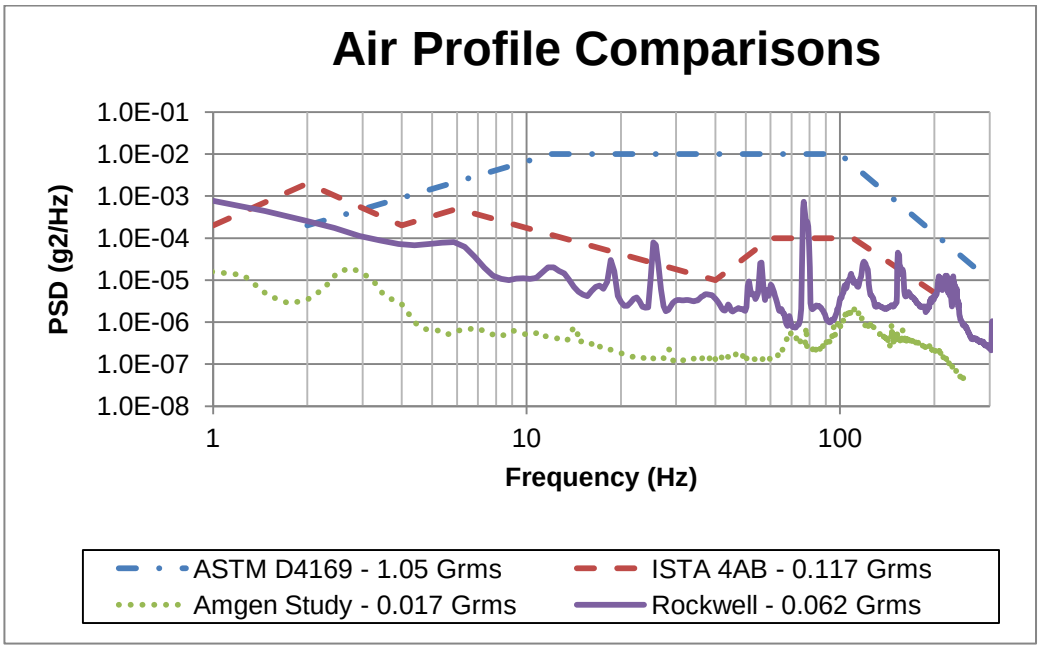

***Figure 1**: Comparison of Air Vibration Profiles*

2.2. Aircraft, Instrumentation and Recording Parameters

The aircraft instrumented for this project was a 1980 Cessna 172 Skyhawk (Figure 2). The engine has a single shaft with a cruising rotational speed of 2500 ± 5% RPM or 41.6 ± 5% Hz throughout the duration of all flights. Data was recorded using a field data recorder with an internal triaxial accelerometer mounted in an unpressurized cargo area, allowing internal atmospheric pressure gauge recordings of actual altitude during flight.

Figure 2: *Cessna 172 Skyhawk*

A Shock and Vibration Environment Recorder, (SAVER™), model 9x30 with SaverXware programming software was used in this study. This data recorder was selected due to the necessity of being able to record vibration and altitude in order to separate in-flight data from ground data.

The data recorder was rigidly mounted to the aircraft's cargo area using a custom aluminum fixture designed specifically for this application (Figure 3).

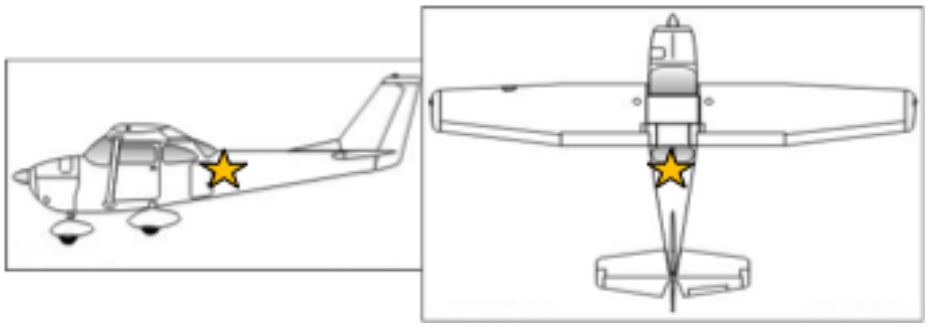

Figure 3: *Location of the Data Recorder (Represented by Star)*

The data recorder was programmed to record and analyze vibration using both signal and timer triggered data collecting methods. Signal triggered data refers to the data recorded during an event in which the intensity exceeds a preset threshold. Timer trigger data refers to the data recorder "waking up" at a preset frequency and recording for a preset duration. The following were the recording parameters used for this project:

- Signal Triggered Data
    - Event Trigger: Threshold: 0.50 G
    - Sample Rate: 1000 Samples/Sec
    - Record Time: 2.048 sec.
    - Signal Pre-Trigger: 20%

- Timer Triggered Data
    - Wakeup Interval: Every 30 sec.
    - Sample Rate: 1000 Samples/Sec
    - Record Time: 2.048 sec.

3. Results and Discussion

A total of 15 individual flights were recorded and analyzed for this project to provide the statistical validity needed to properly characterize the environment. The data was statistically analyzed and mean overall Grms levels were computed.

The flights recorded in this study varied in length from one to three hours. All of the flights were recorded in the Southeastern U.S., with the majority of the flights to destinations located in South Carolina. Some flights experienced the external excitation variables of air turbulence, air pockets, and/ or weather patterns. Interestingly, the internal excitations due to the propellers rotating at 41.6 ± 5% Hz are not visible in the aircraft vibration data (Figure 4). This was possibly due to vibration absorbers built into the engines that absorbed the energy produced at the operating frequency. Table 1 shows the average overall Grms values for the timer and signal trigger data recorded from the fifteen individual flights.

Table 1: *Timer and Signal Trigger Results*

	Timer Trigger (g^2/Hz)	Signal Trigger (g^2/Hz)
Overall Grms	0.110	0.191
Standard Deviation	0.014	0.021

While the maximum accelerations recorded were as high as 1.83g, these levels represented discrete events occurring during takeoffs and landing; whereas the typical steady state vibration did not exceed 0.3g. Not all flights recorded during this study produced signal triggered data. This was due to the aircraft not experiencing any acceleration over 0.50 G during that particular flight.

Figure 4 represents the timer and signal triggered data showing the differences in intensity. Although the two PSD profiles have a similarly shaped curve, the intensity of the signal triggered data was greater than that of the timer triggered data. The average overall Grms level of the fifteen flights for the timer trigger data was 0.110, while the average overall Grms level of the fifteen flights was 0.191 for the signal trigger data.

Figures 5 and 6 display the averaged signal and timer triggered data overlaid with the published breakpoints from Rockwell Twin Engine turbo propeller study. These figures illustrate some of the similarities and differences in the shape of the curves for the data collected in this study with that of Rockwell Twin Engine turbo propeller study. These similarities indicate a similar frequency response of the aircraft measured in the two studies.

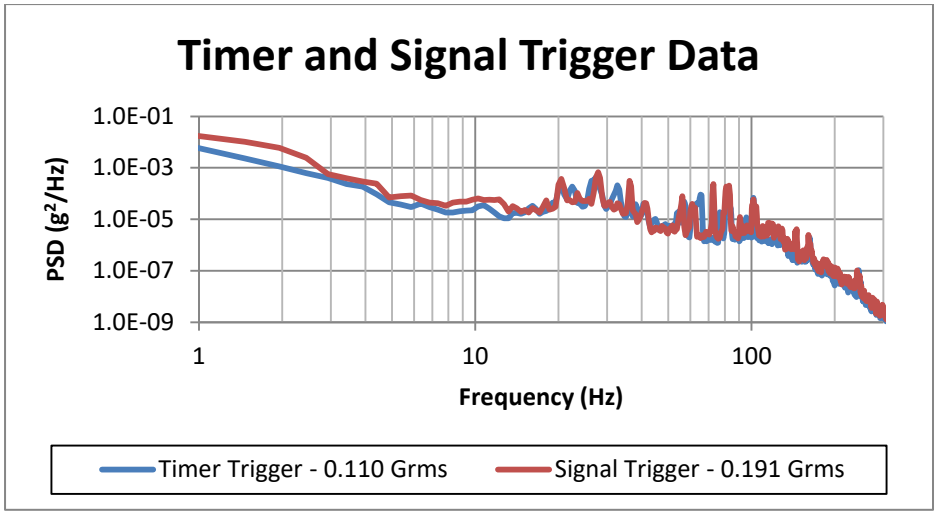

Figure 4: *PSD Profiles for Average Timer and Signal Trigger Data*

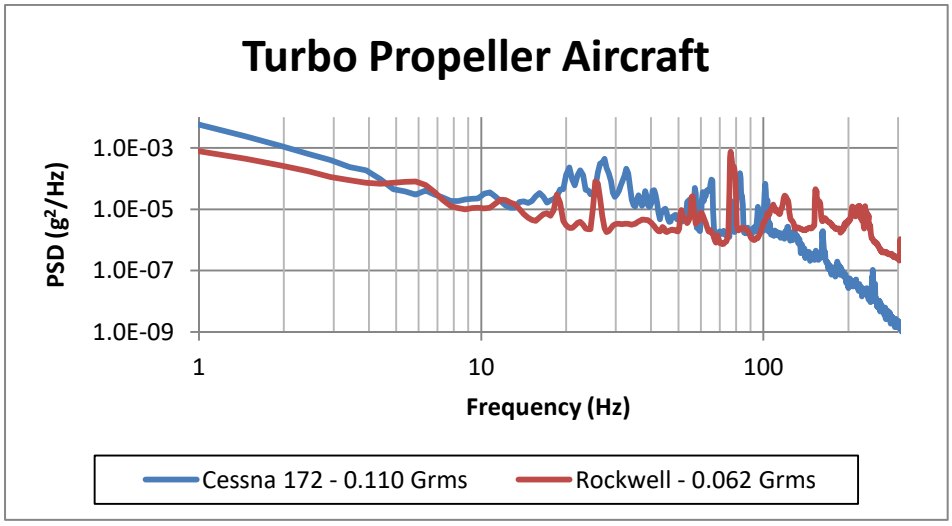

Figure 5: *Averaged Timer Trigger Data for the Cessna 172 and the Rockwell Twin Engine*

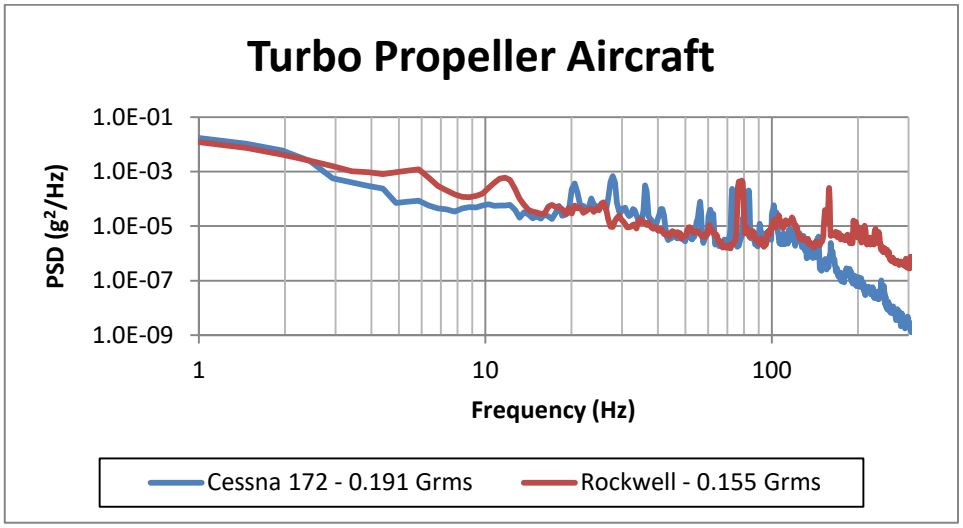

Figure 6: *Averaged Signal Trigger Data for the Cessna 172 and the Rockwell Twin Engine*

4. Conclusions

Recent technological advances in data recording have made it possible to record at a higher sample rate and separate segments of an aircraft's flight using pressure change. Being able to separate these segments makes it possible to individually characterize and analyze a particular aircraft's environment. The analyzed data from the environment and aircraft shows current test methods for aircraft vibration simulations exceed the actual environment for which the simulations are meant to represent. When data from previous studies were compared with that which was collected from this study, the results showed that the ASTM D 4169-09 Air PSD profile exceeds the actual vibration environment.

The maximum accelerations recorded occurred primarily during the ascent and descent of the aircraft. The maximum accelerations recorded were as high as 1.83g. These levels represented discrete events occurring during takeoffs and landings: whereas the typical steady state vibration did not exceed an intensity of 0.3g.

The excitation from the engines rotating at 41.6 ± 5% Hz was not visible on the PSD spectrums. This was believed to be due to vibration absorbers built into the engine producing a smoother, more comfortable ride for the passengers and cargo at typical operating engine speeds.

This method of collecting data could be used to understand the vibration in different aircraft in order to generate vehicle specific vibration profiles. By having multiple vibration profiles exhibiting the random vibrations experienced on an aircraft, the goal of a more optimized package and product system could be met.

References

[1] Trost, T. *Mechanical Stresses on Products during Air Cargo Transportation*. Packag. Technol. Sci. 1988. 1; 137-155.

[2] Ackerman, K.B., 1990: *Practical Handbook of Warehousing*. Third Edition. New York: Van Nostrand Reinhold.

[3] Forest Products Laboratory, 1979: *General Technical Report FPL 22*. Forest Products Laboratory (FPL), U.S. Department of Agriculture. Madison, WI.

[4] UPS Air Cargo, 2007: *Aircraft*. Accessed from http://www.ups.com/aircargo/using/services/services/domestic/svc-aircraft.html.

[5] Singh, S.P., Singh, J., Stallings, J., Burgess, G., and Saha, K. *Measurement and Analysis of Temperature and Pressure in High Altitude Air Shipments*. Packag. Technol. Sci. 2010. 23; 35-46.

[6] ASTM International, 2009: *ASTM D4169 – Standard Practice for Performance Testing of Shipping Containers and Systems*. ASTM, West Conshohocken, PA.

[7] ISTA, 2012: *Resource Book 2012*. ISTA: East Lansing, MI.

[8] Joneson, E., 2006: *Development of Testing Standard for Vibration Simulation*. Proceedings of Dimensions 06. International Safe Transit Association: San Antonio, TX.

[9] Dunno, K., and Batt, G., 2009: *Analysis of In-Flight Vibration of a Twin-Engine Turbo Propeller Aircraft*. Packag. Technol. Sci., 22: 479-485.

[10] Kipp, W., 2008: *ISTA Field Data Requirements*. ISTA: East Lansing, MI.

Cloud Publications
International Journal of Advanced Packaging Technology
2014, Volume 2, Issue 1, pp. 112-118, Article ID Tech-305
ISSN 2349 – 6665, doi 10.23953/cloud.ijapt.13

Research Article **Open Access**

Rice Hulls as a Cushioning Material

Siripong Malasri, Ryne Stevens, Alex Othmani, Mallory Harvey, Ike Griffith, David Guerrero, Matthew Johnson, Michael Kist, Christopher Nguyen, Sebastian Polania, Ashley Qureshi and Yuliana Sanchez-Luna

Healthcare Packaging Consortium, Christian Brothers University, 650 East Parkway South, Memphis, TN, USA

Correspondence should be addressed to Siripong Malasri, pong@cbu.edu

Publication Date: 14 October 2014

DOI: https://doi.org/10.23953/cloud.ijapt.13

Abstract Rice hulls are a by-product of rice production. It is light, bio-degradable, difficult to burn and less likely to allow moisture to propagate. In this study, rice hulls were used as a cushioning material inside a plastic tote. Its impact absorption property was compared to a 3/16-inch bubble wrap and a 0.129-inch anti-vibration rubber pad. From the same baseline, 1-inch thick rice hulls reduced impact acceleration by 25% as compared with 39% and 42% of bubble wrap and anti-vibration pad with the same thickness, respectively. When wet, rice hulls became denser. Thus, the impact increased at the rate of 0.054% per 1% increase of water per hull weight. To make the use of rice hulls practical, rice hulls were placed in sealed plastic bags. Sealed bags containing rice hulls reduced impact acceleration by 41%, which was comparable with the bubble wrap case due to trapped air inside the sealed plastic bag. Using bubble wraps would be more economical and practical. However, bubble wraps could burst and cushioning property would be lost. A sealed plastic bag with rice hulls inside could burst, but the rice hulls would provide another line of protection. In addition, rice hull is a good thermal insulating material and would be useful in protecting some temperature-sensitive products during the distribution by placing bagged rice hulls in all sides of a tote or box.

Keywords *Rice Hulls; Impact Acceleration; Sustainability*

1. Introduction

Agricultural waste products, such as cotton and rice hulls, are sustainable and compostable. Rice hulls have been used as cushioning materials in mushroom packaging [1]. Some other natural

products, such as coconut fiber and wood straw, have been used to prevent damages to papayas and mangoes during the distribution [2]. Banana leaves and Teak leaves were used as wrapping materials for guava while Neem leaves, rice straw, and bamboo leaves were used as cushioning materials for guava fruits during storage [3]. These are examples of the sustainability movement.

Rice hulls are the coating of rice grains. They were removed from raw grains in the making of brown rice. With further milling, white rice was produced. Rice hulls are relatively light with a unit weight of 20-21 pounds per cubic foot [4]. Rice hulls have been used in the production of Portland cement, tooth cleaning substance, beer, fertilizer, and fuel [5].

In this study, the shock absorption property of loose rice hulls was compared with two common cushioning materials, i.e., bubble wraps and anti-vibration rubber pads. The impact property of loose wet hulls and bagged hulls were also investigated.

2. Materials and Methods

Three materials were used in this study; (1) 3/16-inch bubble wrap, (2) 0.129-inch anti-vibration rubber pad, and (3) loose rice hulls, as shown in Figure 1. A 100-g tri-axial shock record was used to measure impact acceleration. It was housed in a single-wall corrugated box. Thick viscoelastic foam was placed at the bottom of the box to ensure the impact accelerations would not exceed the recorder's capacity. This was considered as the study baseline. Each of the three cushioning materials was placed above the viscoelastic foam and underneath the recorder. One-inch thickness of rice hulls was used while up to three layers of bubble wraps and anti-vibration pads were used and results were projected for an one-inch thickness. Figure 2 shows the setup of the shock recorder with 1-inch thick rice hulls over thick viscoelastic foam at the bottom. Viscoelastic foam (the white part in Figure 2) was also used on the sides and top (not shown in Figure 2) to prevent the movement of the recorder. The corrugated box was taped to the bottom of a plastic tote (commonly used in medical device industry) which was dropped at 18-inch drop height as shown in Figure 3. Water was added to loose rice hulls and a similar drop test was performed. Loose rice hulls are hard to handle and not practical. Thus they need to be confined in a container as a unit. In this study rice hulls were placed loosely in plastic bags to obtain different bag thicknesses. An impulse sealer was used to seal these bags. This is shown in Figure 4.

Figure 1: *Cushioning Materials Used in This Study: 3/16-inch Bubble Wrap (left), 0.129-inch Thick Anti-Vibration Pad (center); and Rice Hulls (right)*

Figure 2: *Shock Recorder Setup*

Figure 3: *Plastic Tote and Drop Test*

Figure 4: *Bagged Rice Hulls*

3. Results and Discussion

3.1. Comparing Rice Hulls with Bubble Wrap and Anti-Vibration Pad

First, the tote with the shock recorder attached on thick viscoelastic foam was dropped 20 times. The average impact acceleration was determined to be 77.53g with a standard deviation of 4.12g. The 77.53g was used as a base value. The shock recorder was then placed on 1, 2, and 3 layers of 3/16”

bubble wrap with thicknesses of 0.1875”, 0.375”, and 0.560”, respectively. Twenty drops were made for each case and average impact accelerations were computed as 58.85g, 57.98g, and 53.08g which yielded -24.09%, -25.22%, and -31.54% changes from the base value. These percent changes were plotted against thicknesses and a trend line equation was developed and used to estimate the percent change at 1-inch thickness. The same procedure was used with anti-vibration pads. Two sets of 20 drops were performed with 1” thick loose rice hulls. The average change of the two sets was -24.95%. Results are summarized in Table 1 and Figures 5 and 6. At the same 1-inch thickness, bubble wrap, anti-vibration pads, and rice hulls reduced the impact acceleration by 41.51%, 39.45%, and 24.95%, respectively.

Table 1: *Drop Test Results*

	Base	**3/16" Bubble Wrap**			**Anti-Vibration Pad**			**Rice Hulls**	
Number of Layers		1	2	3	1	2	3	1	1
Thickness		0.1875"	0.375"	0.560"	0.129"	0.258"	0.516"	1"	1"
Average Impact Acceleration	77.53g	58.85g	57.98g	53.08g	66.85g	62.90g	52.28g	57.08g	59.30g
Standard Deviation	4.12g	2.51g	2.57g	2.13g	2.75g	1.41g	2.05g	2.60g	5.06g
% Change from Base Value		-24.09%	-25.22%	-31.54%	-13.78%	-18.87%	-26.13%	-26.38%	-23.52%
Trend Line Equation		y = -31.356x - 10.156			y = -19.971x - 19.481			N.A.	
At x = 1"		**-41.51%**			**-39.45%**			**-24.95%**	

Note: x = thickness (inch), y = change from base value (%)

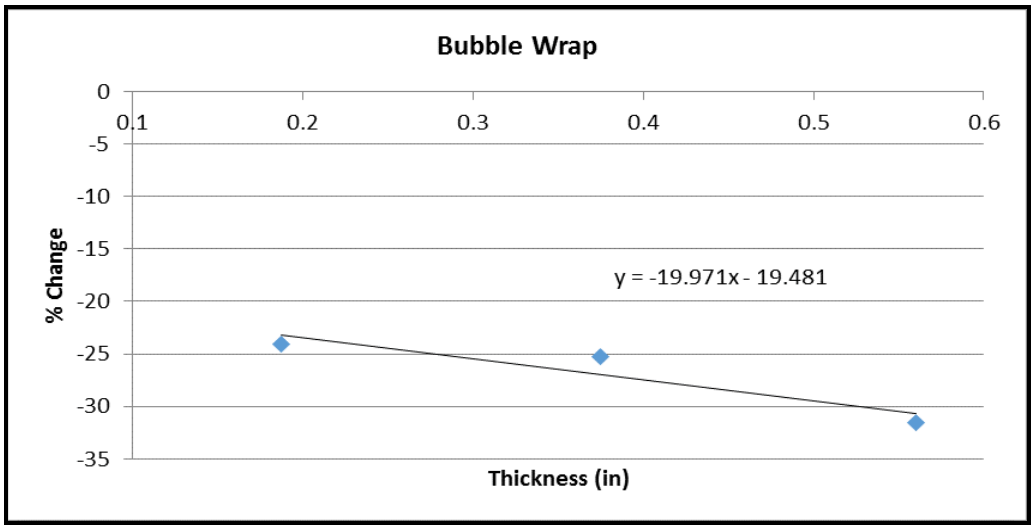

Figure 5: *Drop Test Using Bubble Wrap as Cushioning Material*

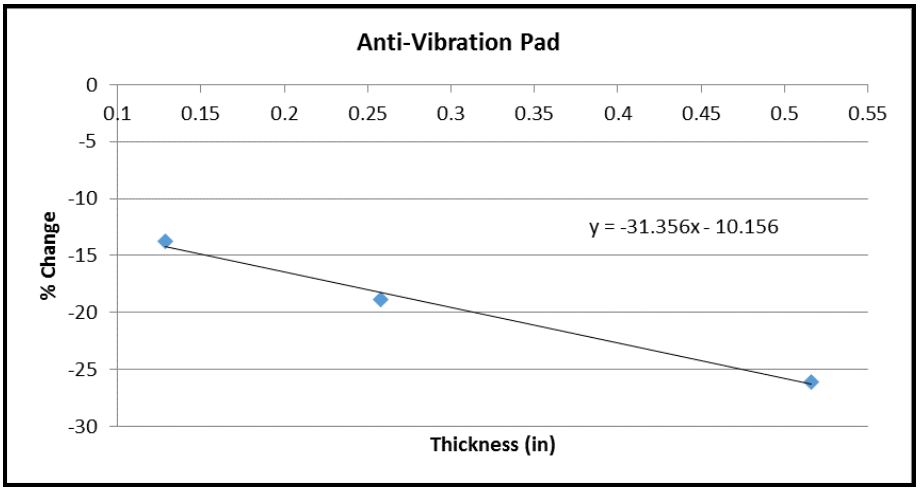

Figure 6: *Drop Test Using Anti-Vibration Pad as Cushioning Material*

3.2. Wet Rice Hulls

When loose rice hulls were subjected to moisture or water, they became denser and the impact absorption ability reduced, as can be seen in Table 2 and Figure 7. As in previous experiments, twenty drops at 18-inch drop height were made for each case. It should be noted that the percentage of water added to the rice hulls were high due to the low unit weight of rice hulls of about 20 pounds per cubic foot compared to much higher unit weight of water of 62.4 pounds per cubic foot. However, the reduction of absorption ability was not significant in most cases, i.e., 13.46% increase in impact acceleration from 0% water to 250% of water per hull weight (or 0.054% increase per 1% increase of water per hull weight). It should be noted that the 0% baseline used in this study was room dry condition at about 50% relative humidity.

Table 2: *Wet Rice Hull Drop Test Results*

Water (% of Hull Weight)	0%	50%	100%	200%	250%
Average Impact Acceleration	57.26g	56.95g	59.16g	61.18g	64.97g
Standard Deviation	5.10g	1.38g	1.55g	1.37g	1.40g

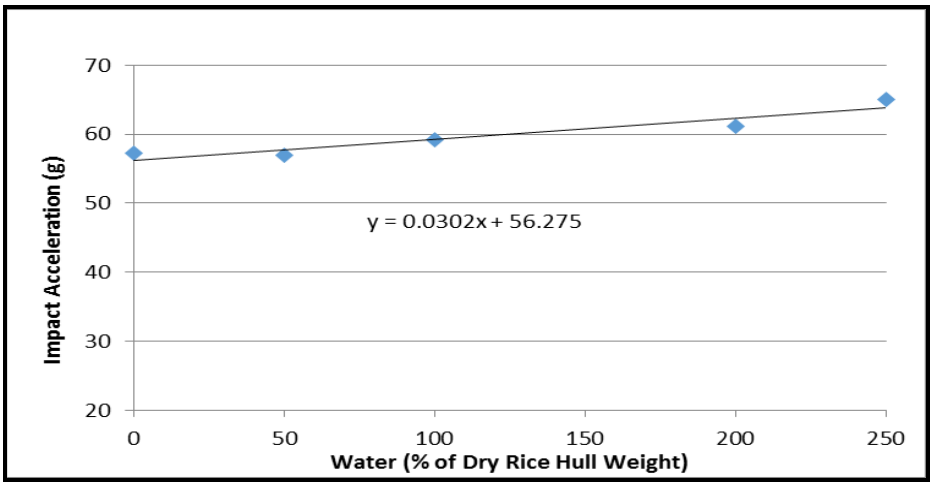

Figure 7: *Wet Rice Hull Drop Test Result*

3.3. Bagged Rice Hulls

For easy handling and waterproofness, rice hulls were placed in sealed plastic bags. These bags were placed under the shock recorder with total thickness of 0.32”, 0.50”, and 0.63”. Twenty drops at 18” drop height were made for each thickness. Results are summarized in Table 3 and Figure 8. From the trend line equation, the change from base value was estimated at -41.04%. This is comparable with the bubble wrap case due to the trapped air inside the bag.

Table 3: *Bagged Rice Hull Drop Test Results*

Thickness of bag(s)	0.32"	0.50"	0.63"
Average Impact Acceleration	77.20g	70.30g	62.45g
Standard Deviation	9.35g	4.19g	2.72g
% Change from Base Value	-0.43%	-9.32%	-19.45%
Equation	y = -60.595x + 19.556		
At x = 1"	**y = -41.04%**		

Note: x = thickness (inch), y = change from base value (%)

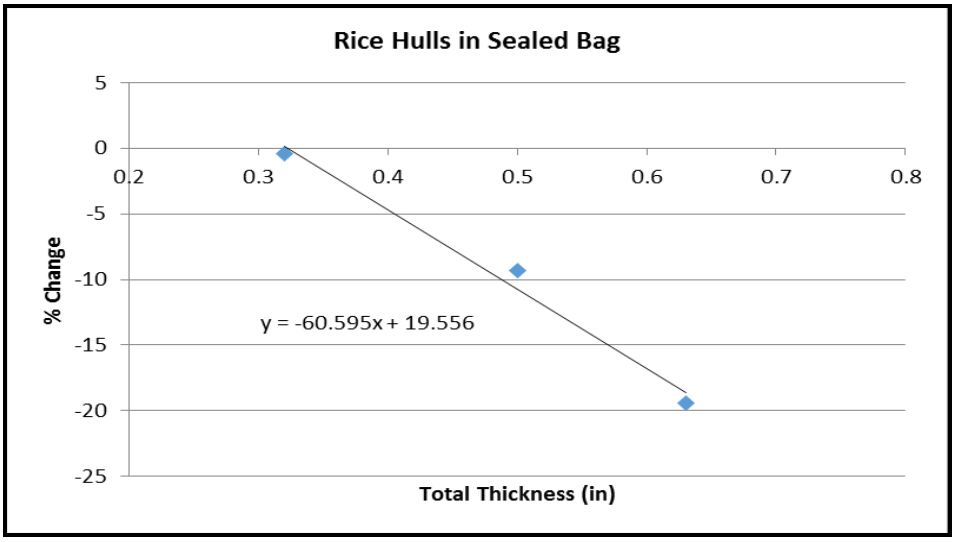

Figure 8: *Bagged Rice Hull Drop Test Result*

4. Conclusion

It was shown in this study that loose rice hulls reduces the impact acceleration about 25% from a base value which was not as effective as bubble wrap and anti-vibration pad. Rice hulls are a natural waste product, which are more environmental friendly than the other two cushioning materials used in this study. However, there are two problems with loose rice hulls:

- They are subjected to moisture, especially if there are liquid product leakages. When wet, they become denser thus less effective in shock absorption.
- They are harder to handle due to its small grain and light weight. In addition they tend to stick to the products inside the tote.

Bagged rice hulls solve the two problems above as well as increase the shock absorption to the level of performance of bubble wrap. When a plastic bag is introduced as part of the solution, the environmental advantage diminishes. In addition, it would be more cost effective in using bubble wrap. However, bagged rice hulls provide double protection when a bag bursts the rice hulls remain

to absorb shock. When bubbles in bubble wrap burst, the shock protection disappears. In addition, rice hulls are a class A insulating material, which are difficult to burn and are more resistance to mold or fungi [5]. Anti-vibration pads are much more expensive and not recommended for this application. Its shock absorption ability is also comparable to much less expensive bubble wrap. The pad was included in this study for comparison purpose only.

References

[1] Elliott, A. *Your Next Gadget Might Be Packaged in … Mushrooms?* Mashable. May 4, 2012.

[2] Castro, C., Faria, J. and Dantas, T. *Evaluating the Performance of Coconut Fiber and Wood Straw as Cushioning Materials to Reduce Injuries of Papaya and Mango during Transportation*. International Journal of Advanced Packaging Technology. 2014. 2 (1) 84-95.

[3] Chandra, D. and Kumar, R. *Qualitative Effect of Wrapping and Cushioning Materials on Guava Fruits During Storage.* HortFlora Research Spectrum. 2012. 1 (4) 318-322.

[4] SCAFCO Grain Systems Co., 2014: *Material Unit Weight*. http://www.scafco.com/upload/userfiles/Grain/Technical_Information/Technical/MaterialUnitWeight.pdf

[5] Wikipedia, 2014: *Rice Hulls*. http://en.wikipedia.org/wiki/Rice_hulls

Cloud Publications
International Journal of Advanced Packaging Technology
2014, Volume 2, Issue 1, pp. 119-128, Article ID Tech-333
ISSN 2349-6665, doi 10.23953/cloud.ijapt.14

Research Article **Open Access**

Shock Absorption of Crumb Rubber and Coconut Fiber

Waleed Alnashwan, Badar Aloumi, Siripong Malasri, Michael Kist, Alex Othmani, Ronald Fotso, Matthew Johnson, Sebastian Polania and Yuliana Sanchez-Luna

Healthcare Packaging Consortium, Christian Brothers University, 650 East Parkway South, Memphis, TN, USA

Correspondence should be addressed to Siripong Malasri, pong@cbu.edu

Publication Date: 27 December 2014

DOI: https://doi.org/10.23953/cloud.ijapt.14

Editor-in-Chief: **Dr. Siripong Malasri**, Christian Brothers University, Memphis, TN, USA

Abstract Millions of scrap tires are generated annually in the United States and threaten the environmental and public health. Coconut fiber is a biodegradable agricultural waste that is plentiful in many tropical countries. Using these two materials would make the world a better place environmentally. Experiments were done to determine the shock absorption properties of these two materials. A 1-inch thick layer of crumb rubber (shredded scrap tires) with four different grain sizes of 6-14 mesh, 10-30 mesh, 50-80 mesh, and 80-200 mesh reduced impact acceleration from a base value by 15.49%, 20.79%, 31.22% and 38.47%, respectively. Crumb rubber with smaller grain size absorbed shock better than crumb rubber with larger grain size. In a similar study, 1-inch thick coconut fiber reduced impact acceleration from the same base value by 46.44%, 41.89% and 36.13% at 0% (room dry), 100% and 200% water contents, respectively. Coconut fiber is more effective in shock absorption when it contains less water.
Keywords *Crumb Rubber; Coconut Fibers; Impact Acceleration; Sustainability*

1. Introduction

Each year, millions of scrap tires are generated in the United State, which threatens the environmental and public health. Scrap tire stockpiles are a breeding grounds for mosquitoes, which results in the spread of dengue fever, yellow fever, encephalitis, West Nile virus, and malaria. Common utilizations of scrap tires include athletic and recreational surfaces, molded and extruded products, rubber-modified asphalt, and tire-derived aggregate [1]. A typical scrap tire contains 70% rubber, 15% steel, 3% fabric, and 12% inert fillers, by weight. Shredded scrap tires with more than 99% of the steel and fabric removed are referred to as crumb rubber [2]. They are sieved into different gradations based on ASTM D5644 [3].

Coconut fiber is a plentiful agricultural waste product in many tropical countries. It has been used to produce more environmentally friendly products; such as, rope, brush, tapestry, automotive parts, gardening products, reinforcing composite, acoustic, thermal insulation, and fruit injury prevention [4]. In a previous study [5], another agricultural waste, rice hull, was used as a cushioning material for plastic tote distribution. A 1-inch thick layer of loose dry rice hulls reduces impact acceleration from a base value by 24.95% comparing with 39.45% and 41.51% of anti-vibration pad and 3/16" bubble wrap of the same thickness, respectively.

In this study, the shock absorption properties of crumb rubber with different grain sizes and coconut fiber with different percent of water contents were compared with those obtained from previous studies [5].

2. Materials and Methods

Crumb rubber with four different gradations: 6-14 mesh, 10-30 mesh, 50-80 mesh, and 80-200 mesh, were used. Their gradations per ASTM D5644 were summarized in Table 1 [6-9] and Figure 1.

Table 1: *Sieve Analysis Data*

	% Retained on Sieve			
	Crumb Rubber Size			
Sieve No.	**6-14**	**10-30**	**50-80**	**80-200**
5	0.0			
6	2.9			
8		0.0		
10	80.2	4.0		
12		20.0		
14	14.9			
16		20.4		
18	2.1			
20		34.8		
30		14.6		
40		4.1	0.0	
50			52.4	
60			15.5	0.7
70			10.9	1.6
80			9.0	18.3
100			4.9	18.8
120			4.0	19.8
140			1.1	8.8
170			1.4	10.7
200			0.9	15.7
Pan	0.0	2.1	0.0	5.6
Total	*100*	*100*	*100*	*100*

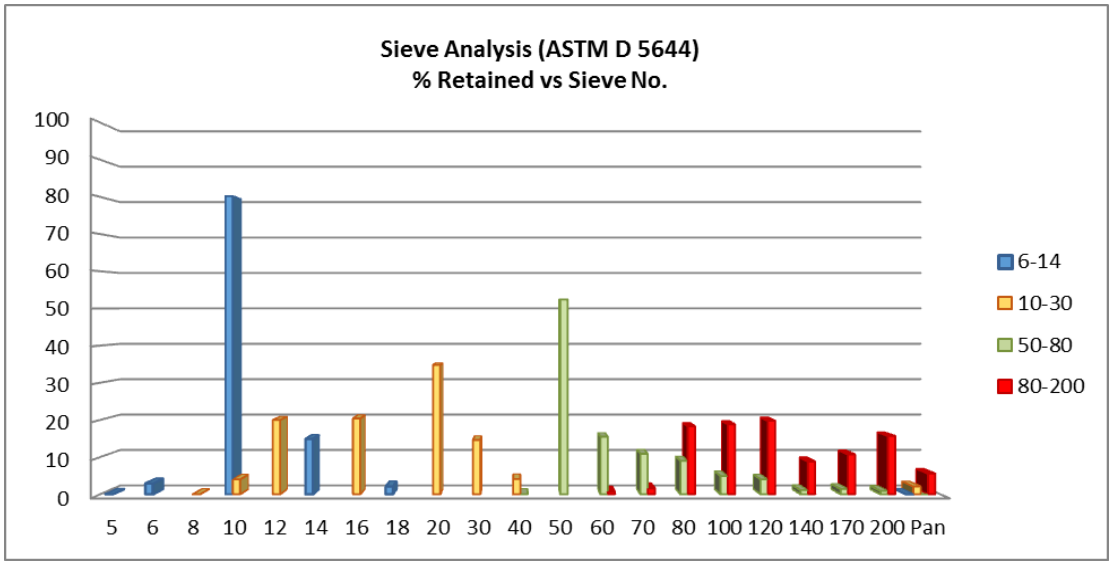

Figure 1: *Sieve Analysis*

One-inch thick sewer-inlet sediment-control coconut-fiber filter, as shown in Figure 2, was used in this study. The fibers are bonded to a fiberglass mesh backing.

Figure 2: *Storm Water Inlet Filter with Plastic Ties*

A 1-inch thick layer of crumb rubber or coconut fiber was placed on a viscoelastic foam base housed in a single-wall corrugated box (Figure 3a). A shock recorder (tri-axial accelerometer) with a 100-g maximum capacity was placed on top of the test material (Figure 3b). The box was then secured tightly to the interior bottom of a plastic tote (Figure 3c). The tote was dropped twenty-five times from an 18-inch height by a drop tester (Figure 3d). Five outlying data points were dropped. This was the same setting used in the previous rice hull study [5]. Thus, the average impact acceleration with shock recorder placed directly on the viscoelastic foam base of 77.53g was used as the base impact acceleration in this study. It should be noted that the viscoelastic foam was used to ensure that the impact acceleration would not exceed the shock recorder's 100g capacity.

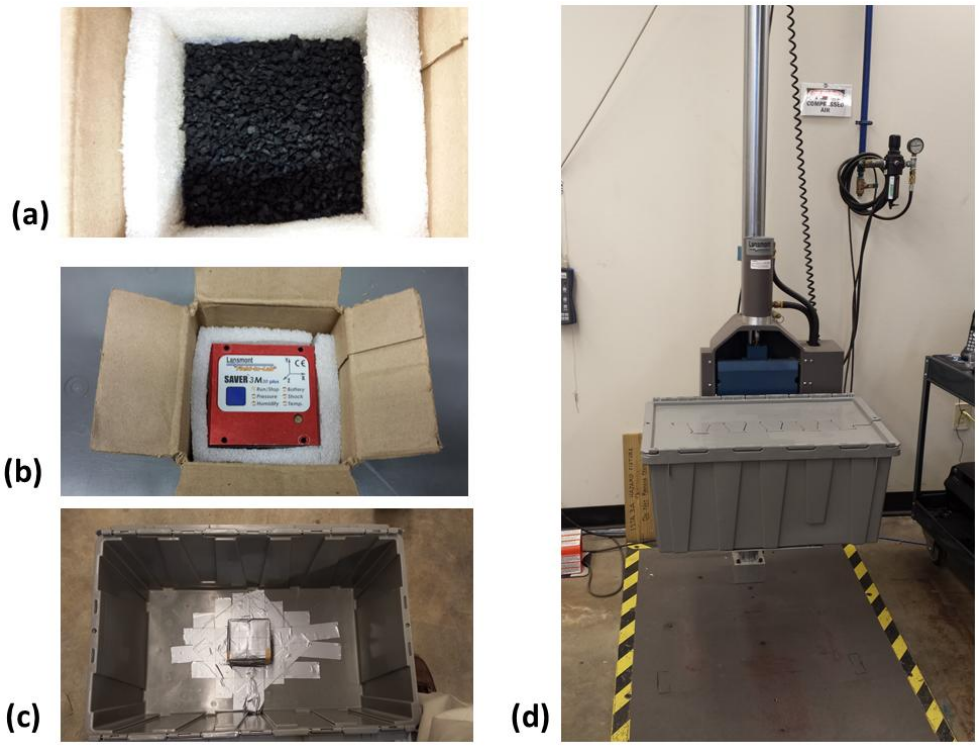

Figure 3: *Experiment Setup*

Bulk density of crumb rubber was based on the weight of crumb rubber that filled a 3”-diameter and 6”-height cylinder.

$$Bulk\ Density\ (pcf) = \frac{Uncompacted\ Weight\ of\ Material\ (lb)}{Volume\ of\ Material\ (ft^3)}$$

In the coconut fiber study, water content was determined based on the room-dry weight.

$$Water\ Content\ (\%) = \frac{(Wet\ Weight - Dry\ Weight)}{Dry\ Weight} X 100$$

3. Results and Discussion

3.1. Crumb Rubber

Data and results of crumb rubber experiment are summarized in Table 2, Figure 4, and Figure 5. The 6-14 mesh had the largest grain size while the 80-200 mesh had the smallest used in this study. The crumb rubber with smaller grain size absorbed more impact because it allowed more particle movements, i.e., better flow. It is also lighter since it contains more voids between particles. It should be noted that loose crumb rubber would not be practical. It would leave dark stains on the product, and thus, it should be bagged. Bagged crumb rubber was not considered in this study since it would yield comparable result as bagged rice hull in previous study [5].

Table 2: *Crumb Rubber Data and Results*

	Impact Acceleration (g)			
Bulk Density (pcf)	31.80	27.72	26.09	21.20
Mesh Size	**6-14**	**10-30**	**50-80**	**80-200**
1	62.26	67.91	48.72	58.05
2	63.59	55.29	47.81	34.24
3	68.28	58.8	48.43	43.99
4	62.52	62.79	47.48	48.2
5	65.68	64.27	49.75	59.55
6	64.16	63.32	57.32	47.27
7	66.56	57.84	53.95	47.12
8	65.34	63.51	52.37	45.54
9	63.71	54.57	50.77	61.58
10	60.91	62.5	53.31	60.73
11	65.46	64.53	51.23	39.67
12	67.20	62.83	58.16	42.68
13	67.19	56.23	59.59	45.11
14	67.00	61.12	56.51	35.37
15	65.28	63.71	50.07	46.97
16	66.64	60.31	54.12	49.69
17	67.23	58.98	54.26	60.28
18	67.47	61.21	59.24	36.23
19	67.30	64.56	53.65	46.28
20	66.67	63.97	59.8	45.54
Avg (g) =	*65.52*	*61.41*	*53.33*	*47.70*
SD (g) =	*2.04*	*3.50*	*4.06*	*8.46*
% Reduction	*15.49*	*20.79*	*31.22*	*38.47*

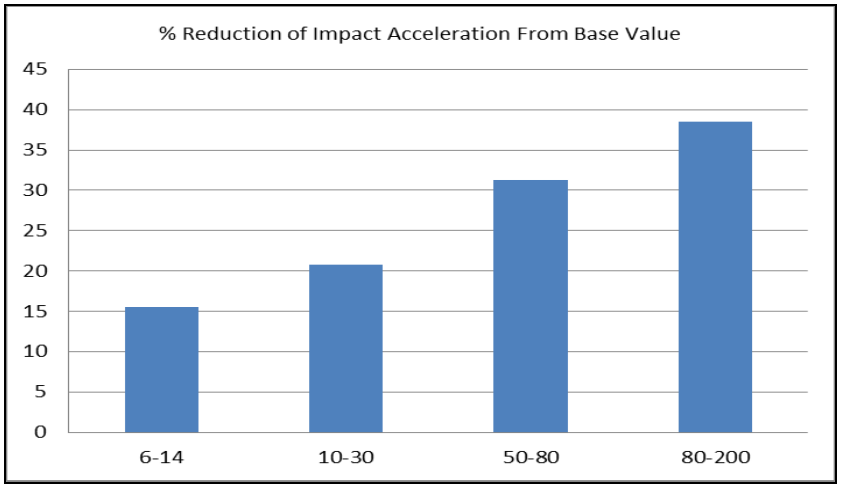

Figure 4: *Impact Reduction versus Crumb Rubber Size*

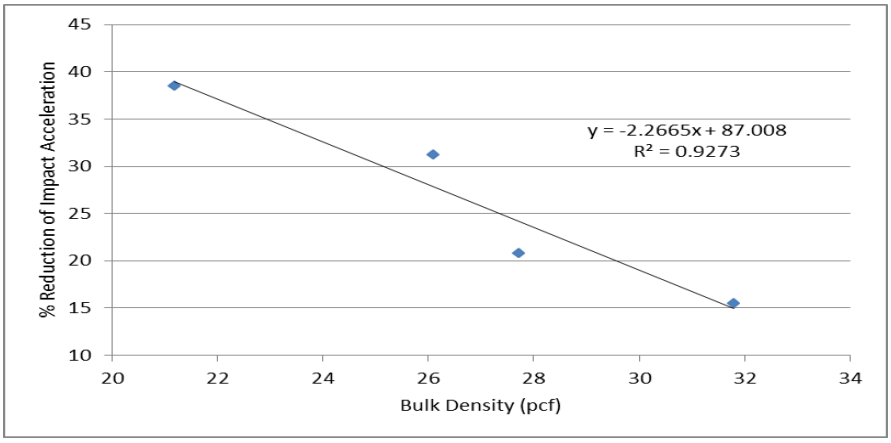

Figure 5: *Impact Reduction versus Bulk Density*

3.2. Coconut Fiber

Data and results of the coconut fiber experiment are summarized in Table 3, Figure 6, and Figure 7. Figure 6 shows that as water content increases, impact acceleration reduction decreases. The wet coconut fiber does not maintain its memory and does not return to its shape before multiple impacts. This phenomenon can be seen in Figure 8. This compression effect makes the coconut fiber denser and lowers its shock absorption ability. This can be clearly seen from Figure 7 in which impact acceleration increases from the 1st to 84th drops. Figure 7 also shows that higher water content makes the fiber denser; thus, it yields higher impact accelerations.

Table 3: *Coconut Fiber Data and Results*

	Specimen A		Specimen B		Specimen C	
Dry Weight (lbs)			0.02			
Wet Weight (lbs)	0.02		0.04		0.06	
Water Content (%)	0		100		200	
Drop No.	Impact Acceleration (g)	Impact Reduction (%)	Impact Acceleration (g)	Impact Reduction (%)	Impact Acceleration (g)	Impact Reduction (%)
1	35.15	54.66	33.58	56.69	45.33	41.53
2	35.42	54.31	34.14	55.97	42.62	45.03
3	30.45	60.72	35.75	53.89	45.03	41.92
4	36.24	53.26	39.14	49.52	47.06	39.30
5	38.08	50.88	38.10	50.86	45.24	41.65
6	36.41	53.04	32.54	58.03	46.43	40.11
7	33.80	56.40	38.94	49.77	47.27	39.03
8	38.60	50.21	39.62	48.90	48.10	37.96
9	36.42	53.02	39.37	49.22	44.23	42.95
10	33.47	56.83	42.02	45.80	47.48	38.76
11	37.27	51.93	45.68	41.08	48.21	37.82
12	38.55	50.28	45.30	41.57	45.04	41.91
13	38.67	50.12	46.14	40.49	44.95	42.02
14	40.28	48.05	40.19	48.16	48.92	36.90
15	41.63	46.30	42.22	45.54	49.31	36.40
16	39.24	49.39	44.33	42.82	48.52	37.42

17	40.98	47.14	45.27	41.61	48.18	37.86
18	40.01	48.39	44.50	42.60	49.33	36.37
19	39.53	49.01	43.58	43.79	49.54	36.10
20	40.21	48.14	44.06	43.17	51.17	34.00
21	43.68	43.66	48.77	37.10	45.97	40.71
22	41.08	47.01	43.09	44.42	51.19	33.97
23	40.14	48.23	44.94	42.04	50.51	34.85
24	38.79	49.97	44.27	42.90	45.22	41.67
25	40.64	47.58	42.18	45.60	50.34	35.07
26	39.59	48.94	44.07	43.16	49.19	36.55
27	39.94	48.48	43.59	43.78	48.01	38.08
28	30.97	60.05	46.75	39.70	44.68	42.37
29	39.78	48.69	42.43	45.27	50.87	34.39
30	30.33	60.88	45.46	41.36	50.23	35.21
31	43.88	43.40	33.31	57.04	50.83	34.44
32	41.96	45.88	50.67	34.64	47.07	39.29
33	39.17	49.48	47.72	38.45	46.01	40.66
34	40.08	48.30	44.37	42.77	51.43	33.66
35	33.13	57.27	47.48	38.76	53.02	31.61
36	43.26	44.20	46.71	39.75	51.54	33.52
37	40.95	47.18	45.93	40.76	51.70	33.32
38	42.00	45.83	46.46	40.07	51.42	33.68
39	40.30	48.02	50.71	34.59	50.64	34.68
40	37.44	51.71	44.63	42.44	40.86	47.30
41	41.96	45.88	49.26	36.46	51.67	33.35
42	44.32	42.84	47.89	38.23	51.45	33.64
43	41.43	46.56	37.94	51.06	49.65	35.96
44	42.41	45.30	48.38	37.60	49.37	36.32
45	40.16	48.20	43.76	43.56	51.18	33.99
46	45.59	41.20	51.21	33.95	48.34	37.65
47	43.49	43.91	49.69	35.91	52.21	32.66
48	45.65	41.12	46.72	39.74	51.80	33.19
49	43.65	43.70	46.75	39.70	51.12	34.06
50	46.37	40.19	34.60	55.37	52.04	32.88
51	43.76	43.56	45.39	41.45	52.92	31.74
52	42.47	45.22	40.65	47.57	44.56	42.53
53	46.10	40.54	46.90	39.51	47.60	38.60
54	46.60	39.89	44.09	43.13	53.77	30.65
55	35.31	54.46	51.30	33.83	47.41	38.85
56	45.45	41.38	47.94	38.17	51.74	33.26
57	37.95	51.05	47.45	38.80	52.14	32.75
58	45.20	41.70	32.82	57.67	53.45	31.06
59	44.28	42.89	42.35	45.38	52.80	31.90
60	45.79	40.94	47.90	38.22	50.17	35.29
61	44.40	42.73	45.59	41.20	52.51	32.27
62	43.52	43.87	52.48	32.31	30.15	61.11

63	46.27	40.32	46.22	40.38	51.24	33.91
64	37.89	51.13	34.86	55.04	51.35	33.77
65	44.66	42.40	48.96	36.85	46.17	40.45
66	46.08	40.56	33.10	57.31	52.54	32.23
67	45.49	41.33	49.76	35.82	50.78	34.50
68	49.38	36.31	51.04	34.17	50.87	34.39
69	44.92	42.06	51.47	33.61	51.88	33.08
70	46.75	39.70	40.03	48.37	52.61	32.14
71	41.85	46.02	49.56	36.08	53.31	31.24
72	40.59	47.65	52.17	32.71	51.13	34.05
73	46.58	39.92	52.67	32.07	53.34	31.20
74	47.58	38.63	49.96	35.56	53.70	30.74
75	45.18	41.73	52.77	31.94	51.56	33.50
76	47.50	38.73	51.77	33.23	52.30	32.54
77	47.86	38.27	50.76	34.53	53.84	30.56
78	43.59	43.78	48.66	37.24	52.87	31.81
79	40.40	47.89	51.42	33.68	50.36	35.04
80	44.01	43.23	51.18	33.99	54.47	29.74
81	42.79	44.81	49.56	36.08	52.97	31.68
82	47.40	38.86	47.86	38.27	45.06	41.88
83	47.67	38.51	50.27	35.16	53.38	31.15
84	50.56	34.79	51.40	33.70	53.01	31.63
Average	*41.53*	*46.44*	*45.05*	*41.89*	*49.52*	*36.13*
SD (g)	*4.38*		*5.39*		*3.70*	

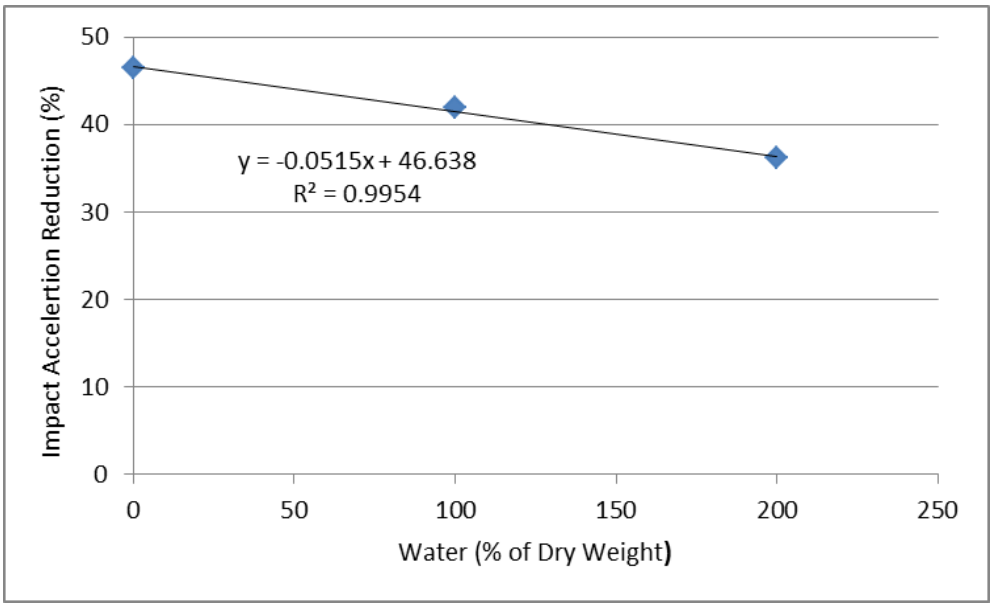

Figure 6: *Average Impact Reduction versus Water Content*

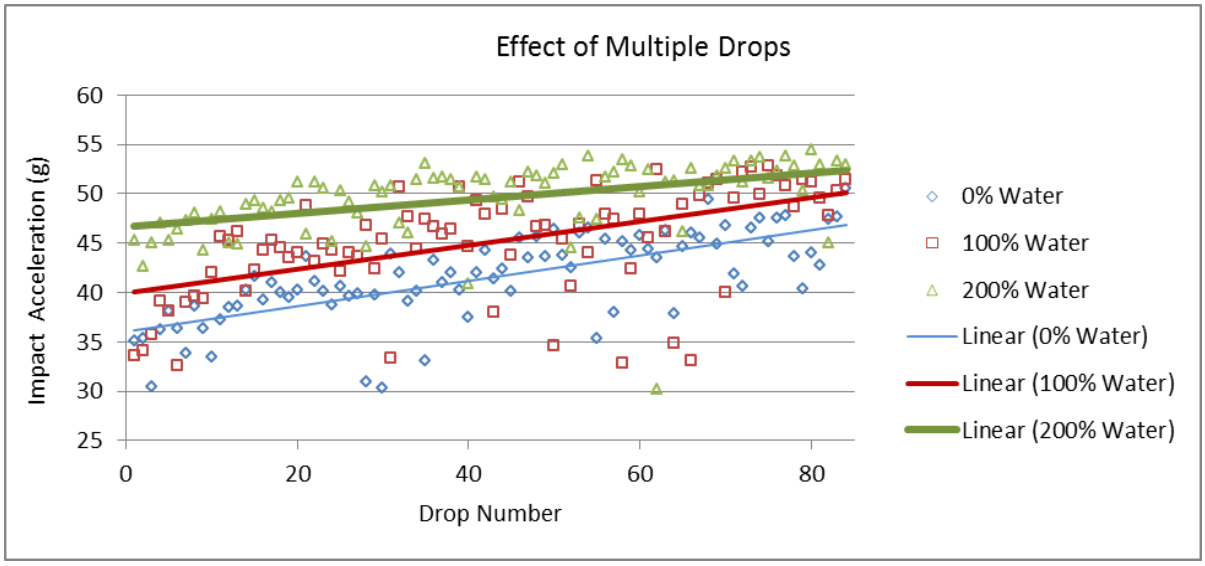

Figure 7: *Effect of Multiple Drops*

Figure 8: *Permanent Deformation of Wet Coconut Fiber*

4. Conclusion

This study showed that loose crumb rubber reduces the impact acceleration from about 15% to almost 40% from a base value depending on the grain size used. Finer grained rubber crumb weighs less and absorbs more impact. The use of loose crumb rubber is not practical because it leaves dark stains on the product. Bagged crumb rubber is highly recommended, which would yield about 40% shock reduction from base value due to trapped air inside the bag similar to bagged rice hull [5]. If a bag was broken, the crumb rubber inside the bag would provide a second line of defense with shock reduction of about 15 to almost 40%.

The coconut fiber, manufactured for storm water inlet filter, is practical since it can be cut to a desire size and is cleaner relative to crumb rubber. When dry, it reduced the impact acceleration by almost 50% from the base value; however, when wet, its impact absorption ability was reduced.

Among the five materials used in this and previous studies, i.e., bubble wrap, anti-vibration pad, rice hull, crumb rubber, and coconut fiber, the coconut fiber stands out as the best choice. It comes in sheet that can be tailored to the container size. It is light and clean (compared to crumb rubber). Most importantly, it provided the best impact absorption ability.

Acknowledgement

Part of the crumb rubber data was presented at the 2014 HPC Fall Meeting (November 2014). Use with permission from Christian Brothers University.

References

[1] United States Environmental Protection Agency, 2010: *Scrap Tires: Handbook on Recycling Applications and Management for the U.S. and Mexico*.

[2] Scrap Tire News, 2014: *Crumb Rubber*. http://www.scraptirenews.com/crumb.php#prettyPhoto.

[3] ASTM International, 2013: *ASTM D5644: Standard Test Methods for Rubber Compounding Materials–Determination of Particle Size Distribution of Recycled Vulcanizate Particulate Rubber*.

[4] Castro, C., Faria, J., and Dantas, T. *Evaluating the Performance of Coconut Fiber and Wood Straw as Cushioning Materials to Reduce Injuries of Papaya and Mango during Transportation*. International Journal of Advanced Packaging Technology. 2014. 2 (1) 84-95.

[5] Malasri, S., Stevens, R., Othmani, A., Harvey, M., Griffith, I., Guerrero, D., Johnson, M., Kist, M., Nguyen, C., Polania, S., Qureshi, A., and Sanchez-Luna, Y. *Rice Hulls as a Cushioning Material.* International Journal of Advanced Packaging Technology. 2014. 2(1) 112-118.

[6] reRubber, 2011: *Sieve Analysis ASTM D 5644: Ambient Crumb Rubber 6-14 Mesh.*

[7] reRubber, 2011: *Sieve Analysis ASTM D 5644: Ambient Crumb Rubber 10-30 Mesh.*

[8] reRubber, 2011: *Sieve Analysis ASTM D 5644: Ambient Crumb Rubber 50-80 Mesh.*

[9] reRubber, 2012: *Sieve Analysis ASTM D 5644: Ambient Crumb Rubber 80-200 Mesh.*

Siripong Malasri, **PhD, PE, CPLP Professional**
Editor-in-Chief, International Journal of Advanced Packaging Technology (ISSN 2349-6665)
Director, Healthcare Packaging Consortium, Christian Brothers University, 650 East Parkway South, Memphis, TN 38104, USA. Phone 1-901-321-3419; Fax 1-901-321-3402; Email pong@cloud-journals.com

Date: December 28, 2014

Dear Readers:

We have reached the end of Volume 2 of the **International Journal of Advanced Packaging Technology**. All articles published in this volume are related to transport packaging, which was the goal we set at the beginning of 2014. In addition the journal has obtained an ISSN number, a major milestone.

On behalf of the journal, I would like to thank the authors for their articles. I would also like to thank the Volume 2 editors, reviewers, and technical assistants:

- M.S.R. Airan, PhD, Cloud Publications, India
- Amit Chauhan, Cloud Publications, India
- Kyle Dunno, PhD, CPLP Professional, Sealed Air, USA
- Jay Gilman, FedEx, USA
- Mallory Harvey, Christian Brothers University, USA
- Lerpong Jarupan, PhD, Kasetsart University, Thailand
- Tunyarut Jinkarn, PhD, Kasetsart University, Thailand
- Eric Joneson, CPLP Professional, Lansmont, USA
- Yong Gang Kang, PhD, Tianjin University of Science and Technology, P.R. China
- Michael Kist, Christian Brothers University, USA
- Shukadev Mangaraj, PhD, Central Institute of Agricultural Engineering, India
- Paul Marshall, CPP, PMP, Smith & Nephew, USA
- Ali Pourhashemi, PhD, Christian Brothers University, USA
- Asit Ray, PhD, Christian Brothers University, USA
- Jose Antonio Rodriquez Tarango, Instituto Mexicano de Profesionales en Envase y Embalaje S.C., Mexico
- Mike Tune, CPP, Bayer Consumer Care, USA
- Yongquan Zhou, CPP, FedEx, USA

Happy New Year 2015,

S. Malasri

Siripong Malasri